Chapter1

Introduction

1.1 Background

Low temperature polycrystalline silicon (LTPS) thin film transistors (TFTs) has been widely investigated as a material for active-matrix liquid-crystal display (AMLCD) applications such as high-definition television, portable devices, and projection displays. Poly-Si TFTs afford the high mobility and the capability of realizing integrated circuits on glass. In recent year, many groups have respect for ambient light sensors, because it may contribute to low power consumption and improve visibility by detecting ambient light around the display panel and controlling the brightness of the display panel. However, the disadvantage is the increase in the volume of the display module and difficulties in the manufacture. Therefore, if we integrate the ambient light sensor with the same LTPS technology used to fabricate the display, the fabrication cost can be reduced, and the process can be simplified.

On the other hand, the photosensitivity of LTPS TFTs is a significant design consideration for achieving high-image-quality display panels since it will affect the leakage current. We should figure out the mechanism of photo leakage current.

1.2 Review of Unit-Lux Current

In order to figure out the photosensitivity effect for poly-Si TFT, Unit-Lux Current (ULC) is a newly introduced parameter to depict the photo induced current. It is used to analyze the effects of illumination on LTPS TFTs.

1.2.1 Definition of Unit-Lux Current

The definition of Unit-Lux Current (ULC) is first described in the paper [1]. We already know that the off current increases with the intensity of the incident light and weak gate bias dependence under high illumination. For different bias conditions, the relationships between drain current and illumination intensity in the off region are shown in Fig. 1-1 [1]. It exhibits good linear dependence between each other. Thus, we define this slope as Unit-Lux Current, (ULC in abbreviation.) which is an important index for analyzing the photosensitivity of LTPS TFTs. The physical meaning of Unit-Lux Current is the photo leakage current induced “per unit-photo flux” and independent of the dark current [1].

1.2.2 Field Effect on Unit-Lux Current

Fig. 1-2 [1] shows how Unit-Lux Current enlarges with drain bias under different gate biases. It is noticed that drain bias affects the photo leakage current in an anomalous way, and different gate biases also causes distinct increments. On the other hand, the change of Unit-Lux Current is not obvious with gate bias under different drain biases.

1.2.3 Anaysis of Unit-Lux Current

From the same report [1], as shown by the arrow line in Fig. 1-2 [1], the linear ULC curve at low drain bias can be fitted, and this is one of the two components of the total ULC. This component which increases with drain bias linearly and independent of gate bias is defined as ULC_{C1}. Then, the second component which subtracts ULC_{C1} from the total ULC curve is called ULC_{C2}. It’s obvious to notice that ULC_{C2} increases with drain bias exponentially when VD is large. Therefore, it is proposed that Unit-Lux Current can be expressed by a linear combination of these two components:

$$\mathrm{ULC} = ULC_{C1} + ULC_{C2} \tag{1.1}$$

$$\mathrm{ULC}_{\mathrm{C1}} = (\alpha \mathrm{VD} + \beta) \tag{1.2}$$

$$\mathrm{ULC}_{\mathrm{C2}} = \gamma \cdot \exp^{(\eta 1 \mathrm{VD} - \eta 2 \mathrm{VG})} \tag{1.3}$$

Where α, β, γ, $\eta 1$, and $\eta 2$ are all fitting parameters. The first term $\mathrm{ULC}_{\mathrm{C1}}$ is proportional to VD and independent of VG. The second term is $\mathrm{ULC}_{\mathrm{C2}}$ which increases with VD and VG exponentially. As shown in Fig. 1-3 [1], this empirical formula agrees with our experiment data very well, which supports our hypothesis that Unit-Lux Current, is composed of two different leakage current components. The values of fitting parameters are also listed in the inset.

Fig. 1-4 [1] shows the ULC in the range of low drain bias is significantly affected by temperature, while that in the higher drain bias range is gradually and less affected by temperature. So the conduction mechanism is proposed to explain the photosensitive effect on the leakage current of LTPS TFT [1]. For the case at low drain bias with light irradiation, when the gate bias is changed, similarly to the abrupt p+n junction, the electric field of the other part in the LDD region is invariable. Thus, the gate voltage independence of $\mathrm{ULC}_{\mathrm{C1}}$ can be explained. As for the Vd effect, the lateral depletion region increases linearly with drain bias. The conduction mechanism of the leakage current in the low drain field is thermal emission. On the other hand, for the high drain bias with light irradiation, the electric field across the lateral depletion region is large enough to fully deplete the LDD region. Therefore, the increase of drain voltage will increase the electric field within the limited LDD length pinched by the n+ region. In such a case, the more negative gate bias will also result in a larger field with the same depletion width of the LDD region. The conduction mechanism of the leakage current at the high drain voltage is field-enhanced emission in the space-charge region.

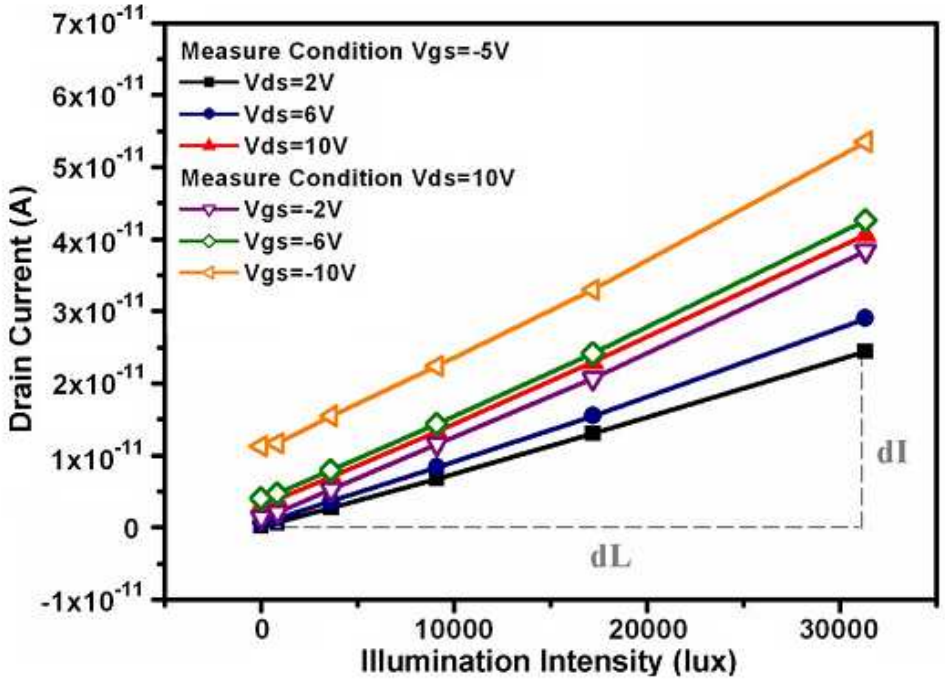

Fig. 1-1. Relationship between leakage current and illumination intensity under different bias conditions.

[*IEEE Trans. Electron Devices*, vol. 56, no. 1, pp. 50-56, 2009.]

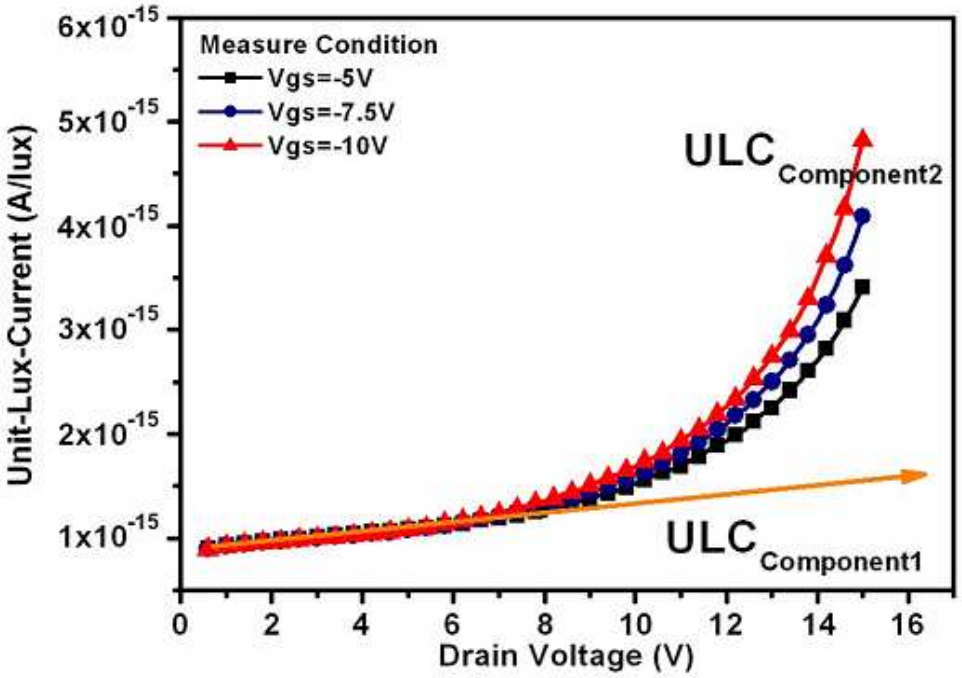

Fig. 1-2. Drain bias effect on Unit-Lux Current at different gate biases.

[*IEEE Trans. Electron Devices*, vol. 56, no. 1, pp. 50-56, 2009.]

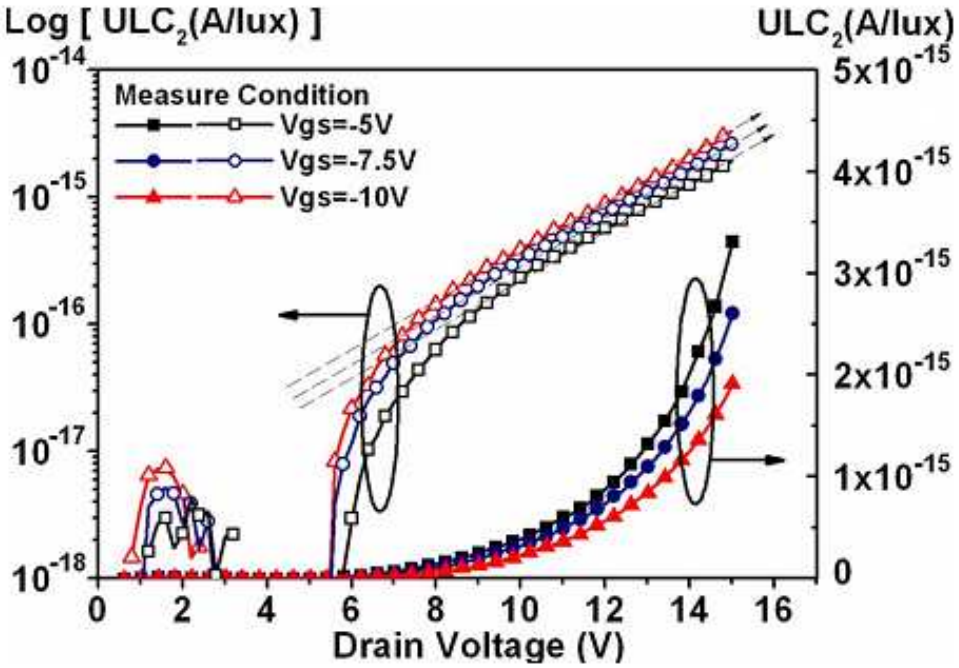

Fig. 1-3. Second component of ULC (ULC2) versus drain bias at different gate voltages.

[*IEEE Trans. Electron Devices*, vol. 56, no. 1, pp. 50-56, 2009.]

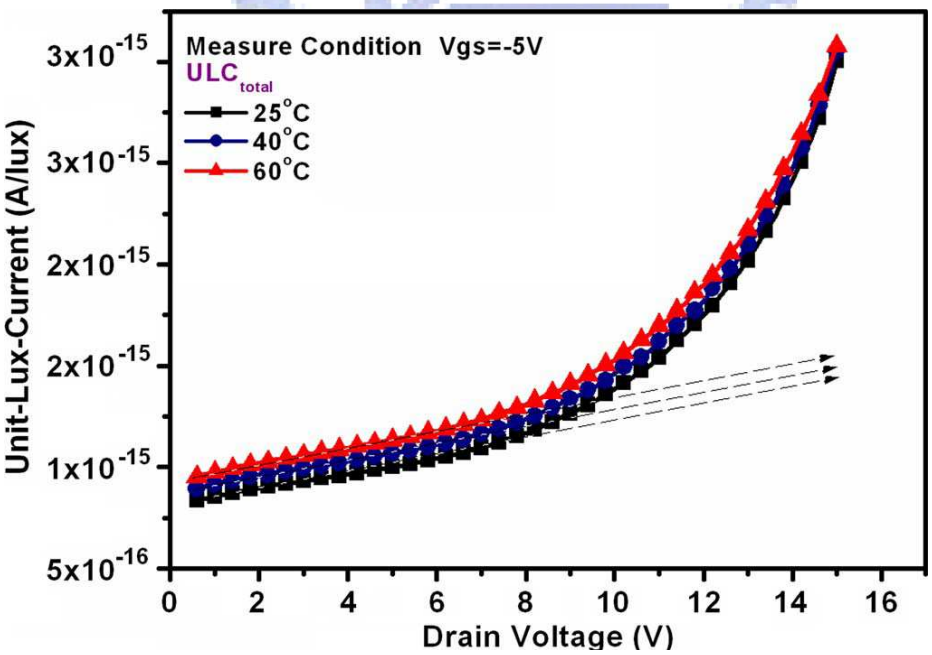

Fig. 1-4. Drain bias dependence of ULC at different temperature

[*IEEE Trans. Electron Devices*, vol. 56, no. 1, pp. 50-56, 2009.]

1.3 Motivation

However, under the consideration of applying LTPS TFTs on light sensing, we know Unit-Lux Current is a new index for defining photosensitivity, In order to understand the characteristics of ULC further, we will explore the major factors that influence ULC via more experiment. In this thesis, first, we confirm that the photo leakage current occurs mainly on the drain side. We also will modify the empirical formula for ULC. The newly revised formula even more conforms to well describe the photo induced current under the measure condition of defect states, and temperature. Finally, we will analyze the effects of defects and discuss the mechanisms of ULC_{C1} and ULC_{C2} respectively.

1.4 Thesis Organization

Chapter 1 Introduction

1.1 Background

1.2 Review of Unit-Lux Current

1.2.1 Definition of Unit-Lux Current

1.2.2 Field Effect on Unit-Lux Current

1.2.3 Analysis of Unit-Lux Current

1.3 Motivation

1.4 Thesis Organization

Chapter 2 Sensing Area Consideration

Chapter 3 Effects of Defects

3.1 Defects Created by Hot Carrier Stress

3.1.1 Review Degradation Mechanism and Experiment Content

3.1.2 Photo Current Variation after Stress

3.1.3 Analysis Unit-Lux Current after Stress

3.1.4 Variation of Fitting Factors

3.2 Defects Created by Self Heating Stress

3.2.1 Review Degradation Mechanism and Experiment Content

3.2.2 Photo Current Variation after Stress

3.2.3 Analysis Unit-Lux Current after Stress

3.2.4 Variation of Fitting Factors

3.3 Comparison and Discussion the Mechanism of ULC

Chapter 4 Effects of Temperature

4.1 Unstressed

4.1.1 Analysis Unit-Lux Current

4.1.2 Variation of Fitting Factors

4.2 Case of Hot Carrier Stress

4.2.1 Analysis Unit-Lux Current.

4.2.2 Variation of Fitting Factors.

4.3 Case of Self Heating Stress

4.3.1 Analysis Unit-Lux Current.

4.3.2 Variation of Fitting Factors.

4.4 Summary

Chapter 5 Conclusions

Appendix

References

Chapter2

Sensing Area Consideration

Some previous paper [2, 3] reported that the electron-hole pairs generated by irradiation in depletion region. Therefore, we can surmise that the most sensitive part inside LTPS TFTs to the illumination is at the drain side. We design two experiments for verification. First, we use two different types of TFT. The only distinction is one have unilateral LDD length, the other have bilateral. Fig. 2-1 shows the IDVG curve contract between unilateral LDD length and bilateral LDD length at VD=6V. It makes no big difference of the photo leakage current when both kinds of TFT are conducted based on the same background of measurement process.

The second experiment is exploited a special layout of the TFT with U-shaped source and drain electrode configuration, as shown in Fig. 2-2. Twenty-five TFTs are arranged in parallel and separated into two groups. Each size of TFT is W=20 um, L=8um. The inner electrodes (about 33-μm distance) of the TFTs in these two groups are shorted together and so are the outer electrodes (about 59-μm distance) to form the U-shaped TFT. An irradiation optical beam with 25-μm light spot radius has been used to directly shine on the device. By scanning the beam along the channel direction of the U-shaped TFT, the leakage currents of the LTPS TFT are measured in two cases with the inner or the outer electrodes as drain. As shown in Fig. 2-3, two anomalous peaks of the off current are observed. When the measurement is performed with outer electrodes as drain, the distance is larger (about 66 μm). On the other hand, when the inner electrodes are used as the drain, the distance is shorter (about 32 μm). The distance between the pair peaks is consistent with the device's real junction distance.

Two experiments above reveal the fact that the photo-induced current occurs at drain side only. Hence, the following discussion of the mechanism of Unit-Lux Current will focus only on the drain region.

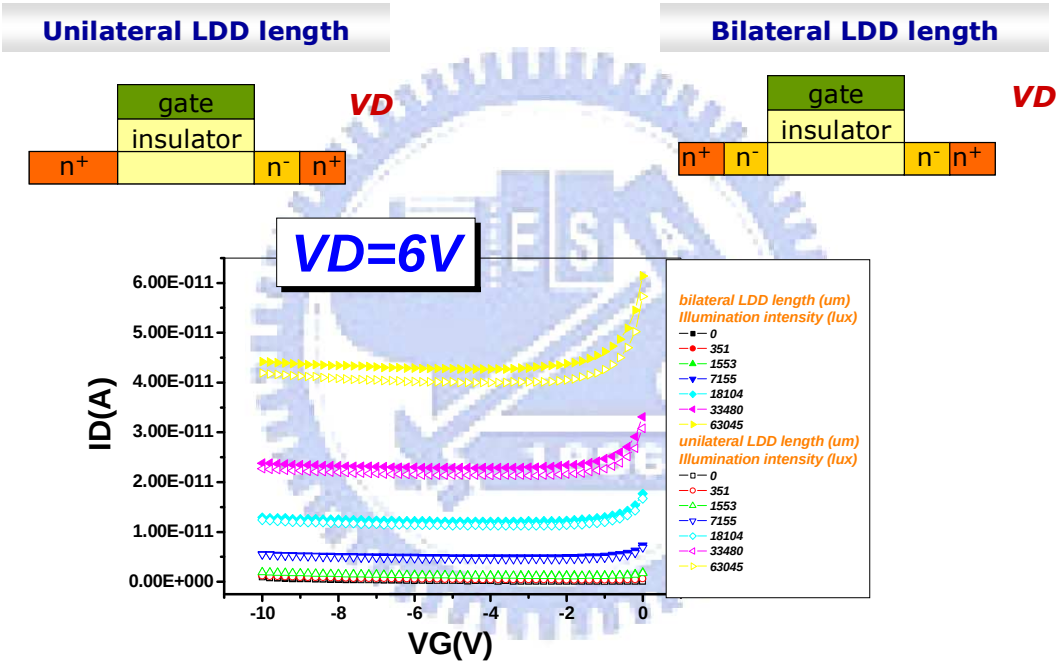

Fig. 2-1 The IDVG curve contract between unilateral LDD length and bilateral LDD length.

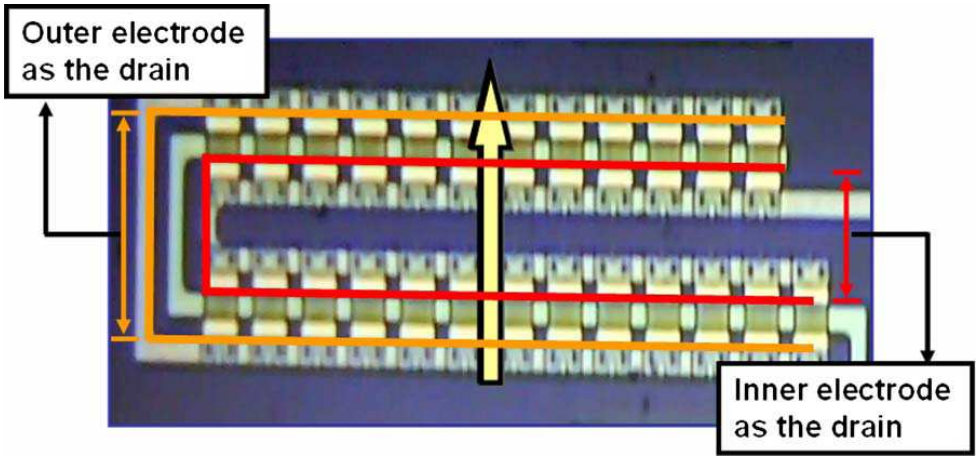

Fig. 2-2 A special layout of the TFT with U-shaped source and drain electrode configuration.

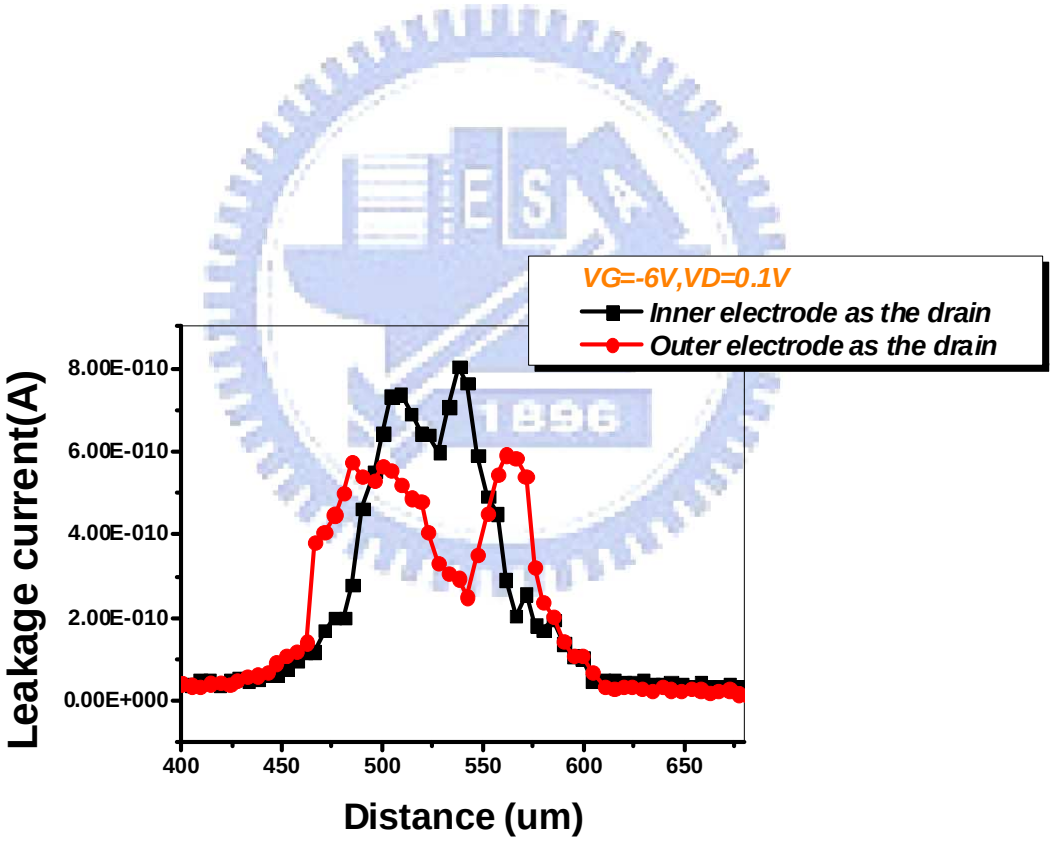

Fig. 2-3 Drain current of the U-shaped TFT with the distance of the illumination beam scanned along the channel direction

Chapter3

Effects of Defects Creation

3.1 Defects Created by Hot Carrier Stress

3.1.1 Review of Degradation Mechanism and Experiment Content

Degradation of the electrical characteristics due to hot carrier (H.C) effect is an important issue in TFTs circuit application. Extensive investigations have shown that hot carrier induced defect states could be generated at the grain boundaries close to drain junction [4].

When a gate bias slightly greater than threshold voltage and a large drain bias applied on a TFT, high electric fields from the voltage difference between gate and drain will present in the junction depletion region. This field accelerates the electron-hole pairs to “hot carriers” with high kinetic energy and strike the lattice structure in this region. Avalanche multiplication due to impact ionization takes place at the drain end of the channel, thus leaves large amount of tail state strain bond defects here.

This degradation phenomenon causes severe decrease on the device mobility, as shown in Fig. 3-1. ID-VG curves at VD=0.6V, 5.3V, 10V after stress altered significantly in both on and off region, and the leakage current increased because the defects act as a transient transfer center for carriers conducting, In the on region, however, these defects trap carriers would decrease the amount of carriers which are collected by drain electrode.

In our experiment, we stressed our devices at VG = 3V, and VD = 12V, and

measured at different stress times of 1, 5, 25, 100, 500, 1000 sec to investigate the variation of Unit-Lux Current owing to the created defects. Table3.1 list the experiment conditions in detail.

3.1.2 Photo Current Variation after Stress

Fig. 3-2 shows photo leakage current measured at VG = -5V, VD = 10V after different stress times. We can find that the photo leakage current rises with the increase in stress time. The variation of ULC with different H.C stress times measured at VG=-5V thereby is shown in Fig. 3-3. It appears that the total ULC is lifted up with the stress times, but the photo-induced current seems to decrease under the high drain bias. We will elaborate this phenomenon in detail in the next section.

3.1.3 Analysis Unit-Lux Current after Stress

As mentioned in the very first of introduction, an empirical formula for fitting Unit-Lux Current was previously proposed [1].In this thesis, we find that the previous empirical formula is not universally correct for all the cases in our experiments. In order to discuss the change of Unit-Lux Current after stress, we slightly modify the empirical formula. The new empirical formula will provide better fitting results for the various behaviors of ULC. The modified ULC also can comprise two components:

$$\mathrm{ULC} = ULC_{C1} + ULC_{C2} \tag{3.1}$$

$$\mathrm{ULC}_{\mathrm{C1}} = A1 \cdot \left\{ \exp^{\mathrm{b1(VD - VDx)}} - 1 \right\} + X \tag{3.2}$$

$$\mathrm{ULC}_{\mathrm{C2}} = A2 \cdot \exp^{(-nVG)} \left\{ \exp^{\mathrm{b2(VD - VDx)}} - 1 \right\} \tag{3.3}$$

A1, A2, b1, b2, X, n are all fitting parameters. *A1* and *A2* are the scaling factor of ULC_{C1} and ULC_{C2}, respectively. *b1* and *b2* are parameters corresponding to the effect of drain voltage, and the drain bias is relate to per unit depletion area. We will discuss

the effect of ULC after DC stress which reflects to the parameter *A1*, *A2*, *b1* and *b2* in section 3-1-4 and 3-2-4.

n is related to the VG effect on ULC_{C2}. *VDx* is the drain voltage reflecting the boundary of ULC_{C1} and ULC_{C2}. *X* represents the ULC at VD = VDx. As shown in Fig. 3-4, the curves calculated by the modified empirical formula agree with the experiment data very well. The values of fitting parameters are listed in the inset of Fig. 3-4.

Fig. 3-5(a) shows the variation of ULC_{C1} at VG=-5V with different H.C stress times. We find that ULC_{C1} is lifted up continually when the stress time is longer. On the contrary, in the case of ULC_{C2}, the more stress time, the greater decrease in ULC_{C2} at VG=-5V as shown in Fig. 3-5(b). In the next section, we will analyze this variation by the fitting factors for ULC_{C1} and ULC_{C2} from the new empirical formula.

3.1.4 Variation of Fitting Factors

In order to further discuss the causes that lead to the different behavior of ULC_{C1} and ULC_{C2} after H.C stress, the fitting parameters are extracted from Fig. 3-5. Fig. 3-6 shows the fitting factors of ULC_{C1}versus stress time. As shown in Fig. 3-6(a), *A1* is severely degraded in the early five seconds. The parameter *b1* related to drain bias is massively increases. The parameter *X* also rises after stress times. *VDx* is the voltage at the boundary of ULC_{C1} and ULC_{C2}. The boundary voltage is somewhere around 6.3V before stress. As shown in the figure, the value hardly changes when stress time increased. Therefore, we will further look into it in section 3-3.

Fig. 3-6(b) shows the fitting factors of ULC_{C2} at VG=-5V. As shown in parameter tendency, *A2* is reduced considerably to almost zero in the early five seconds. This tendency reminds us the similar behavior of the effective mobility after H.C stress [5]. We can observe that the tendency of *A1*, *A2* and effective mobility are

all strongly degraded before the stress time of 100 seconds. The time for the parameter *A1*, *A2* to drop seventy percent is 25 seconds, which is almost the same as that of the effective mobility. This phenomenon hints us that the parameter *A1* and *A2* might be closer related to the factors which can influence the effective mobility.

The related drain bias parameter *b1* is massive increased with stress time and so is *b2*. It is assumed that the increase of drain bias will widen the depletion region for VD<6.3V and than enhance the electric field for VD>6.3V. The model represents the change of *b1* and *b2* on ULC_{C1} and ULC_{C2} as shown in Fig. 3-7. We know that electron-hole pairs generated by light illumination are separated by the large field in the depletion region to make the photo current. Consequently, we infer that the parameter *b1* and *b2* may correspond to the generation of carrier in depletion region. *n*, the parameters related to gate bias, is linearly increase with stress time. It also implies the VG dependent field in the depletion that plays an important role in ULC_{C2}.

Based on the behaviors of ULC_{C1} and ULC_{C2}, we infer that the rise in ULC_{C1} is attributed to the increase of *b1* and *X*, while the decline in ULC_{C2} results from the vanishment of *A1*. Associating the variation in different parameters with that in ULC leads us to understand the mechanism of ULC.

Consequently, we will further look into it in section 3-3.

DC stress	Condition :
Hot Carrier Stress	VG=3(V), VD=12(V), VS=0(V) Stress time = 0, 1, 5, 25, 100, 500, 1000 (sec)
Self Heating Stress	VG=14(V), VD=14(V), VS=0(V) Stress time = 0, 1, 5, 25, 100, 500, 1000 (sec)

EXPERIMENT	Gate Bias (V)	Drain Bias (V)	Illumination Intensity (lux)
VG step VD sweep	-5	0.6 ~ 12 Interval: 0.4071V	0 1566 5940 14486 26460 51300
	-7.5		
	-10		
VD step VG sweep	-2~ -10 Interval:0.4V	0.6	
		5.3	
		10	

Table 3-1 Experiment conditions for DC stress and VD, VG effects on photo leakage.

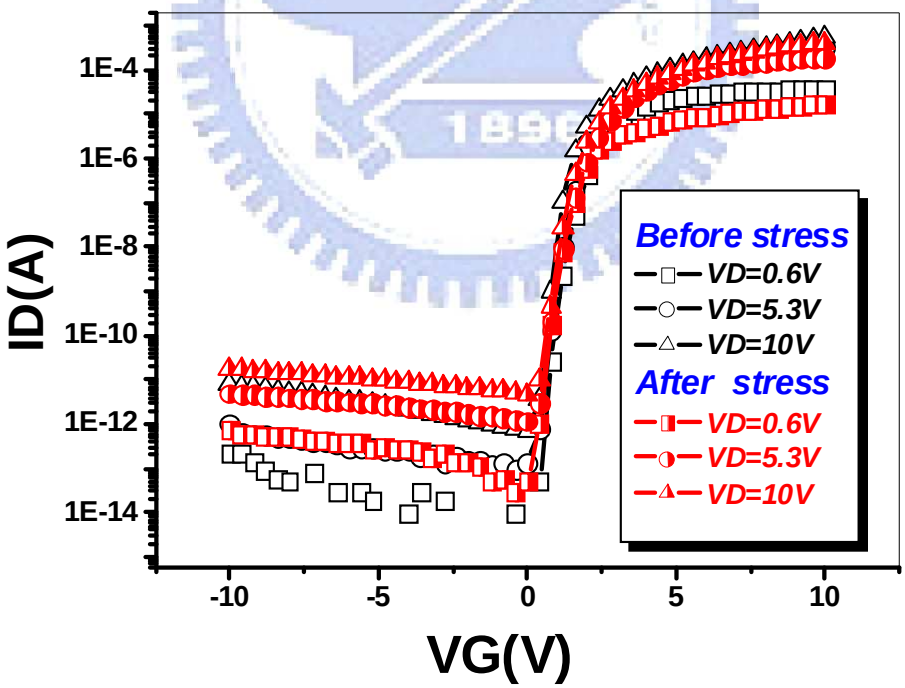

Fig. 3-1 ID-VG curves before and after Hot Carrier stress.

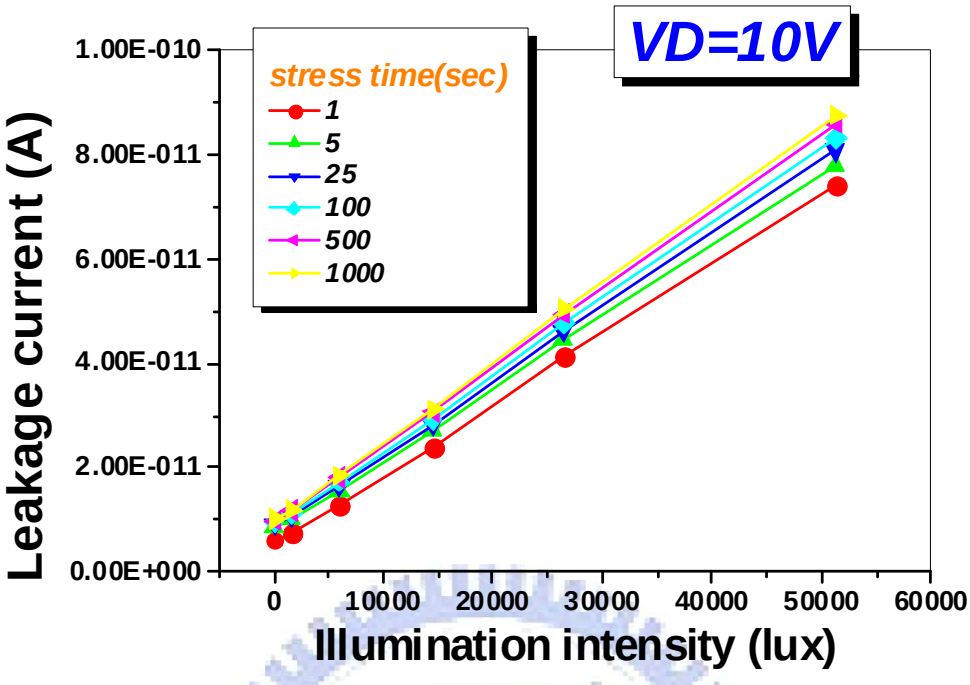

Fig. 3-2 Relationship between leakage current and illumination intensity after different Hot carrier stress time.

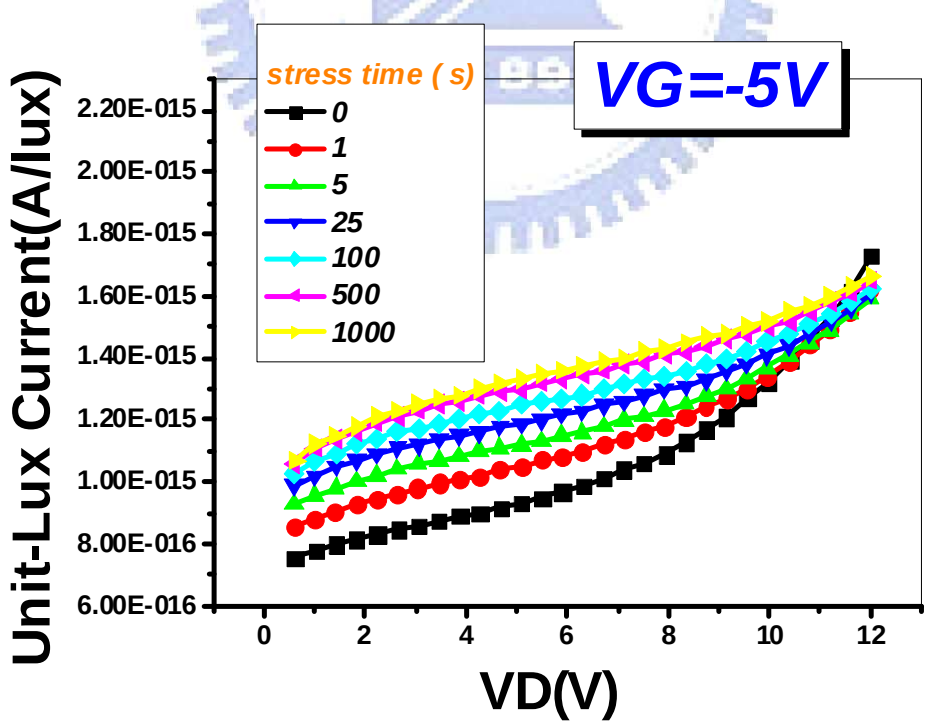

Fig. 3-3 Drain bias dependence of ULC at different H.C stress times.

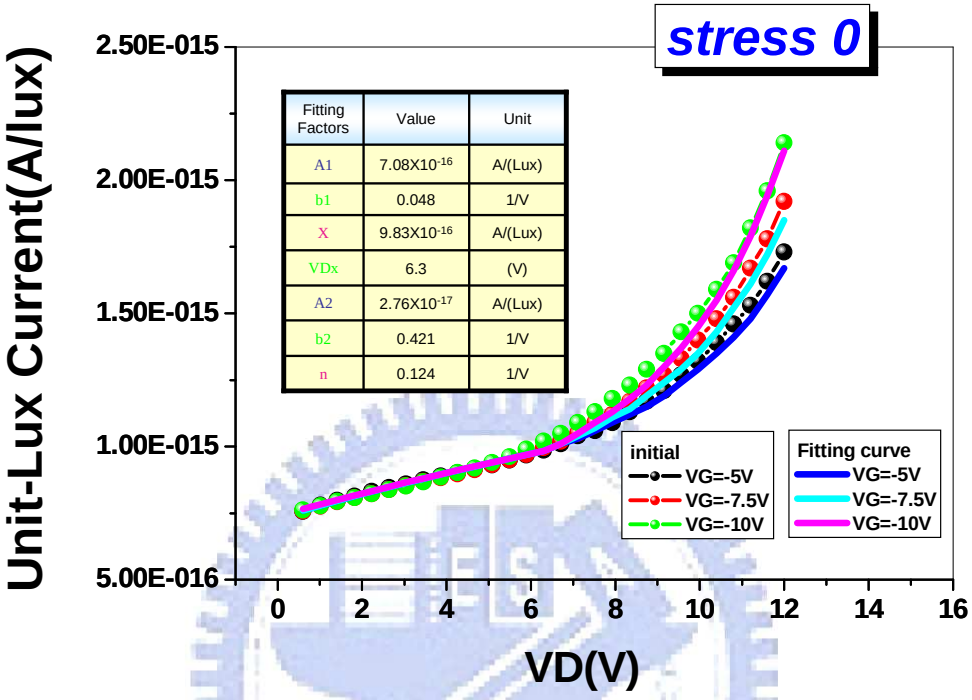

Fig. 3-4 Experiment data (symbols) and empirical formula (solid lines)

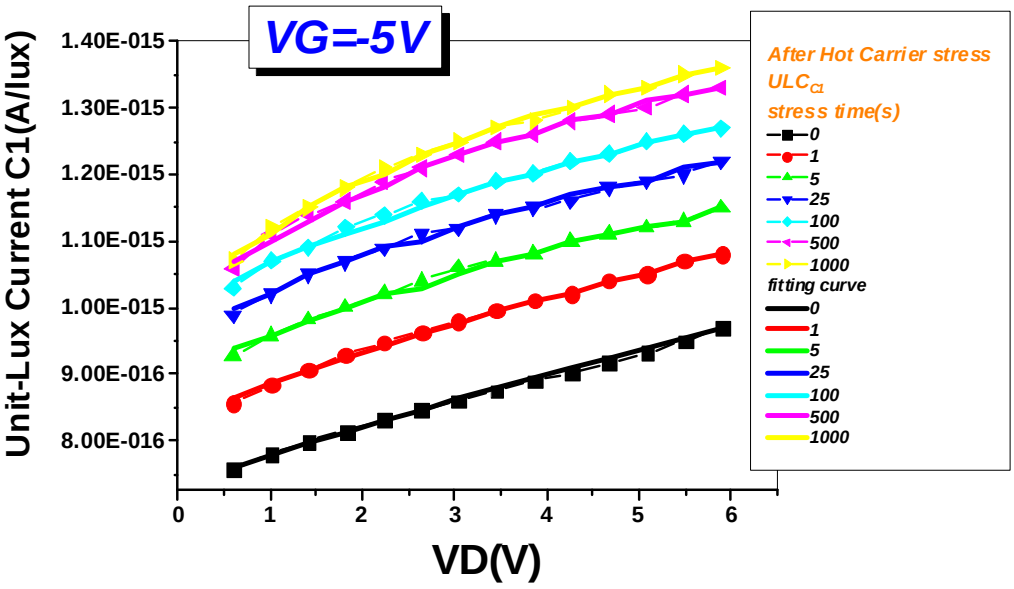

Fig. 3-5(a) The variation of ULC_{C1} versus VD at different H.C stress times.

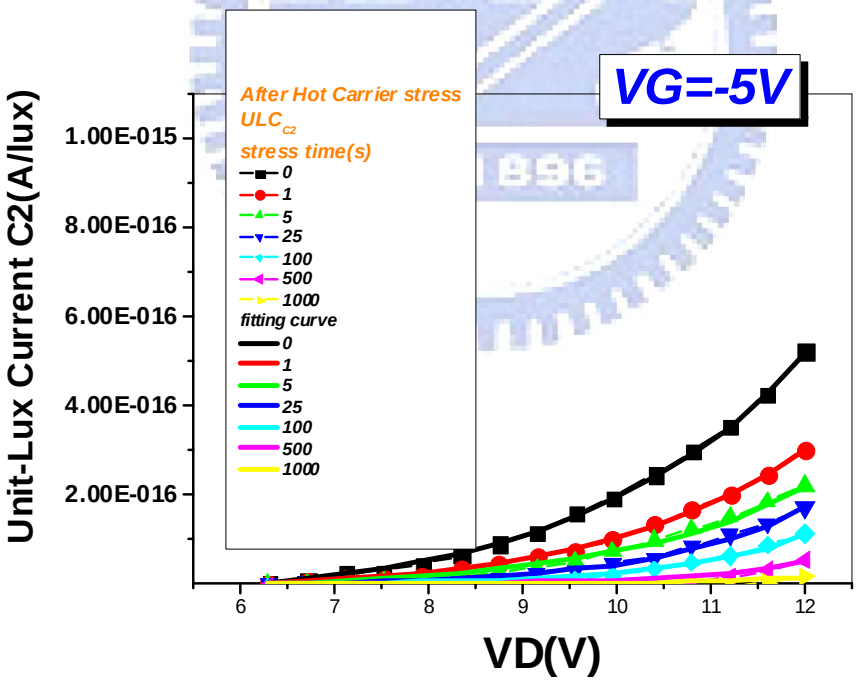

Fig. 3-5(b) The variation of ULC_{C2} versus VD at different H.C stress times.

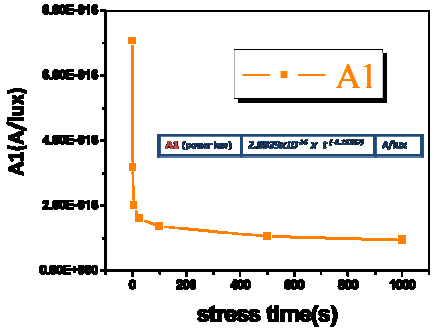

(a)

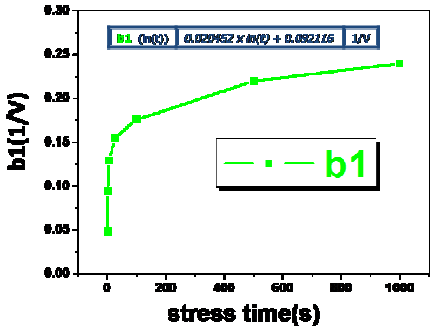

(b)

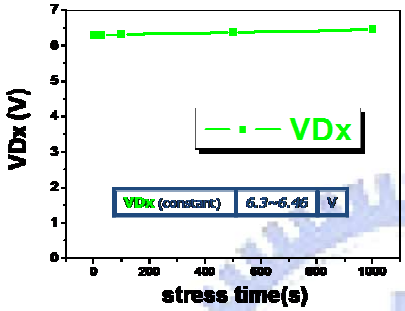

(c)

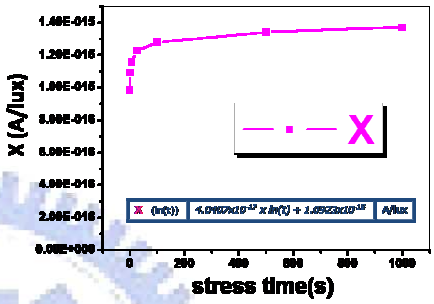

(d)

Fig. 3-6(a) The variation of ULC_{C1} fitting factors (a) A1 (b) b1 (c) VDx (d) X versus VD at different H.C stress times.

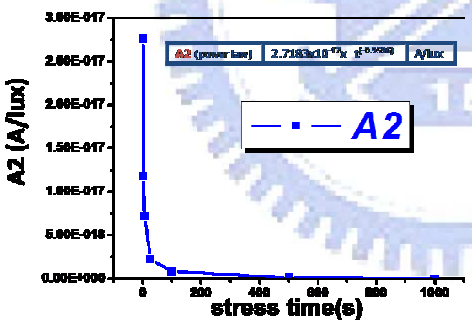

(a)

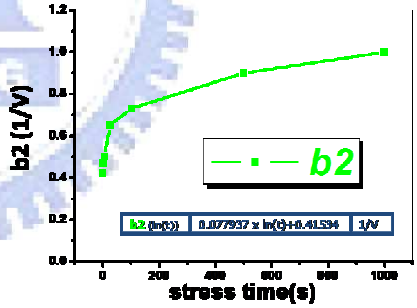

(b)

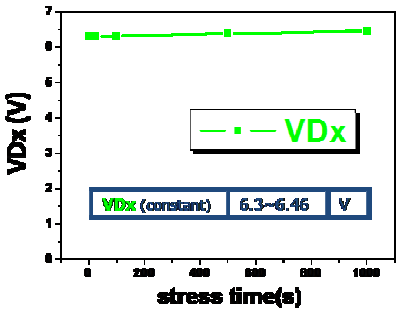

(c)

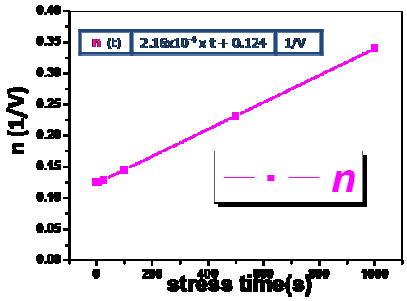

(d)

Fig. 3-6(b) The variation of ULC_{C2} fitting factors (a) A2 (b) b2 (c) VDx (d) n versus VD at different H.C stress times.

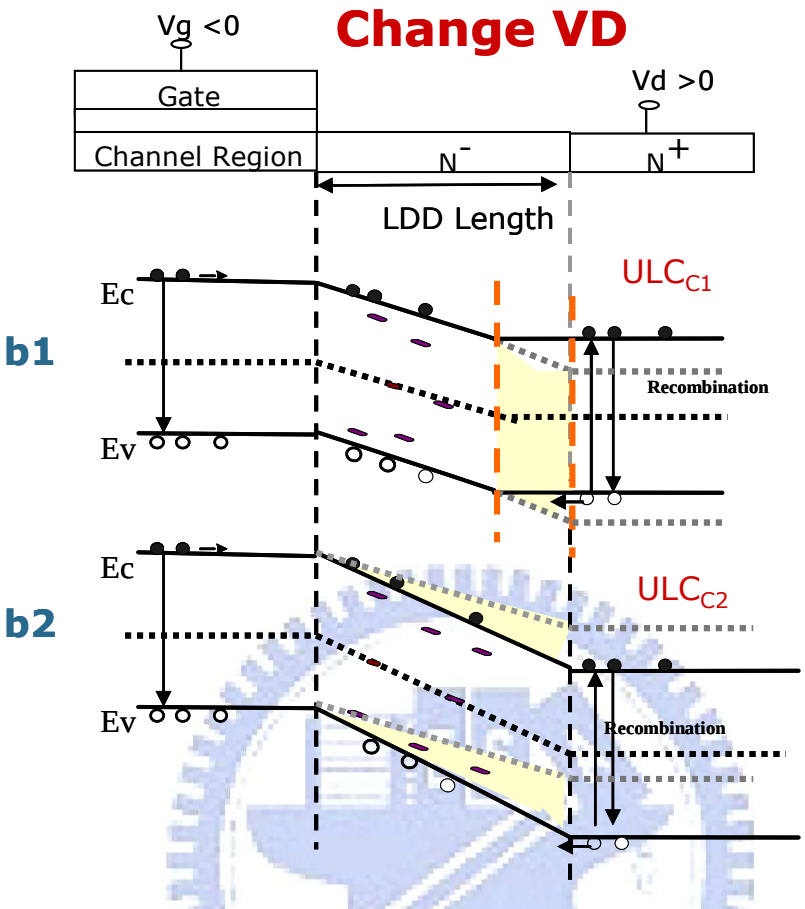

Fig. 3-7 The model represents the change of *b1* and *b2* on ULC_{C1} and ULC_{C2}

3.2 Defects Created by Self Heating Stress

3.2.1 Review of Degradation Mechanism and Experiment Content

LTPS TFTs, in most applications, are fabricated on glass substrates with poor thermal conductivity. Therefore, as the applied V_{GS} and V_{DS} are high, the heat resulting from the high current flow and voltage difference in the channel may be difficult to dissipate. The accumulated heat causes the Si–H bonds to break, which in turn increases the deep states dangling bond in the channel. This degradation is known as Self Heating effect [6].

The states created by self heating stress apparently affect the transfer characteristic of the device mainly in on- and sub-threshold region. Fig. 3-8 is the IDVG curve at the VD = 0.6, 5.3, 10V after self heating stress. Except the lower mobility, serious threshold voltage shift is the most important feature of self heating stress. The physical meaning is that there are numerous deep states in the mid gap to be filled before the device is turned-on.

In our experiment, we stressed our devices at VG = 14V, and VD = 14V, and measured at different stress times of 1, 5, 25, 100, 500, 1000 sec to investigate the variation of Unit-Lux Current.

3.2.2 Photo Current Variation after Stress

Fig. 3-9 shows photo leakage current measured at VG = -5V, VD = 10V after different stress times. We can find that the variation of the photo leakage current with the increase in stress time is slightly. The ULC measured at VG=-5V with different S.H stress times thereby is shows in Fig. 3-10. It appears that the ULC is decreased with the stress times. We will elaborate this phenomenon in detail in the next section.

3.2.3 Analysis Unit-Lux Current after Stress

Fig. 3-11(a) shows the variation of ULC_{C1} at VG=-5V with different S.H stress times. We find that ULC_{C1} is decreased continually when the stress time is longer. On the contrary, in the case of ULC_{C2} at VG=-5V as shown in Fig. 3-11(b). The decrease is slightly with the increase in stress time. In the next section, we will analyze this variation by the fitting factors for ULC_{C1} and ULC_{C2} from the new empirical formula.

3.2.4 Variation of Fitting Factors

In order to further discuss the causes that lead to the different behaviors of ULC_{C1} and ULC_{C2} after S.H stress, the fitting factors are extracted from Fig. 3-11. Fig. 3-12 shows the fitting factors of ULC_{C1} versus stress times. As shown in Fig. 3-12(a), *A1* which might be influenced the effective mobility is degraded in the early five seconds. The parameter *b1* related to the generation of carrier per unit depletion area is decreases, and the parameter *X* also decreases after stress times. *VDx* is the voltage at the boundary of ULC_{C1} and ULC_{C2}. The boundary voltage is equal somewhere around 6.3V before stress. The value hardly changes when stress time increased.

Fig. 3-12(b) shows the fitting factors of ULC_{C2} at VG=-5V. As shown in parameter tendency, *A2* is degraded slightly after S.H stress. The related drain bias parameter *b1* is also decreased. *n*, the parameters related to gate bias, is almost not changing.

Based on the behaviors of ULC_{C1} and ULC_{C2}, we infer that the rise in ULC_{C1} is attributed to the increase of *A1*, *b1* and *X*, while the decline in ULC_{C2} probably has something to do with the sharp decline in *A2*, *b2* and *n*.

. Associating the variation in different parameters with that in ULC leads us to understand the mechanism of ULC.

Consequently, we will also further look into it in section 3-3.

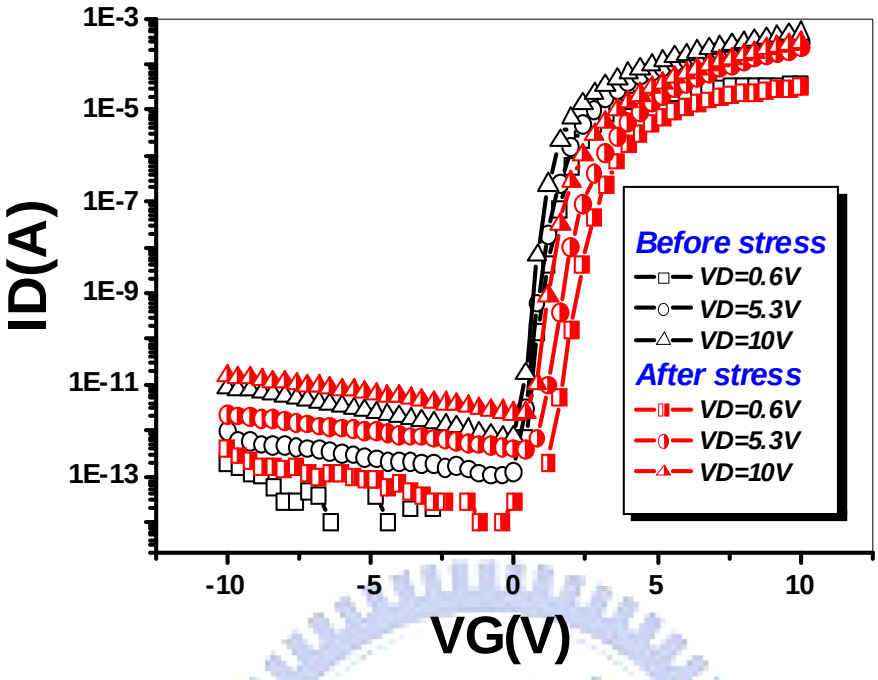

Fig. 3-8 ID-VG curves before and after Self heating stress.

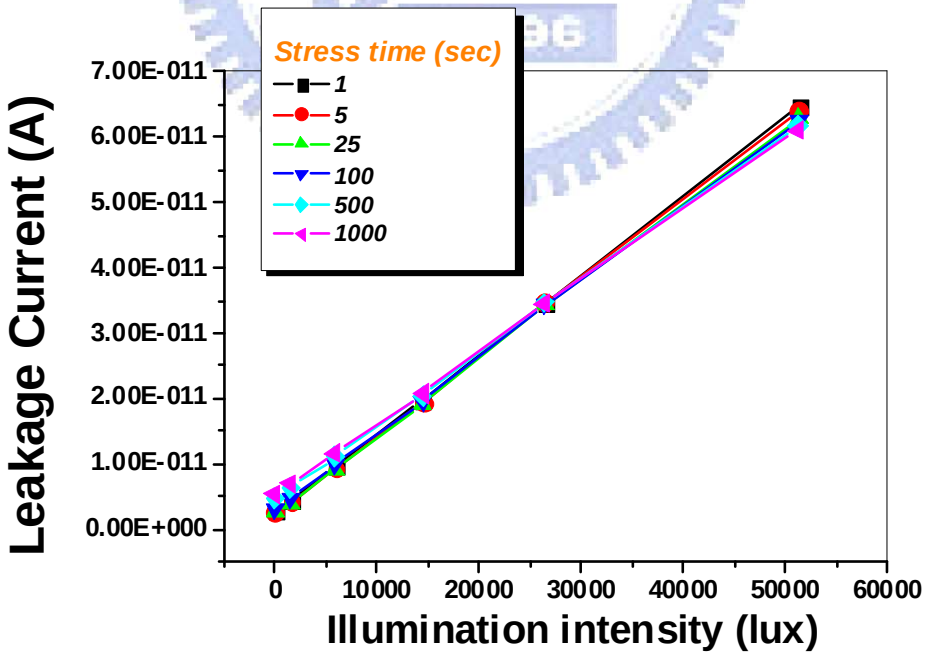

Fig. 3-9 Relationship between leakage current and illumination intensity after different Self heating stress times.

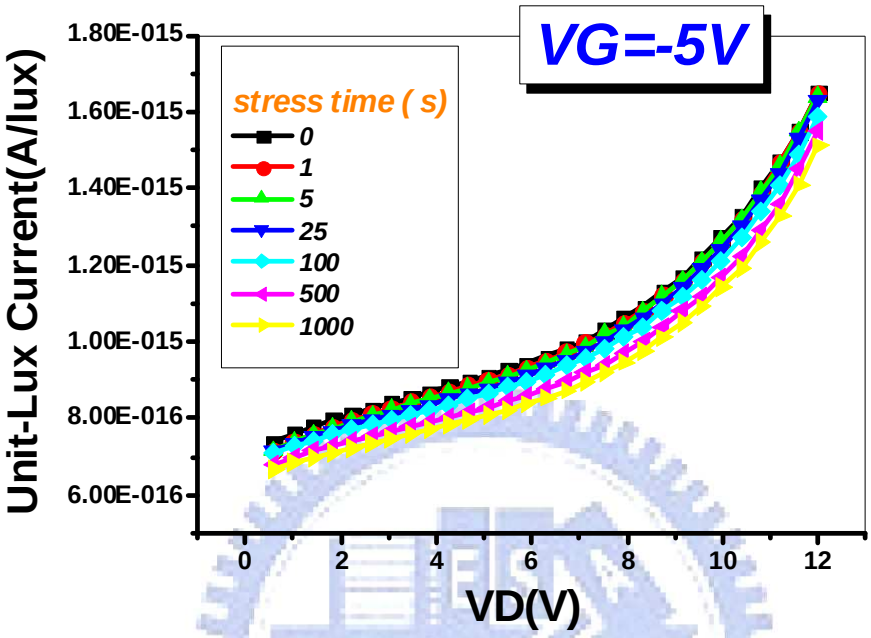

Fig. 3-10 Drain bias dependence of ULC at different S.H stress times.

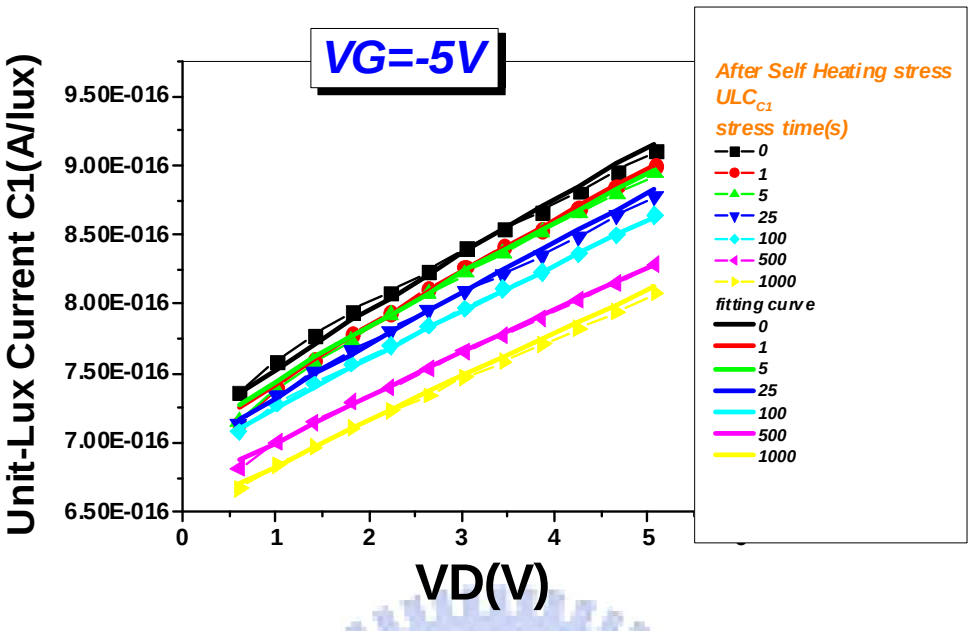

Fig. 3-11(a) The variation of ULC_{C1} versus VD at different S.H stress times.

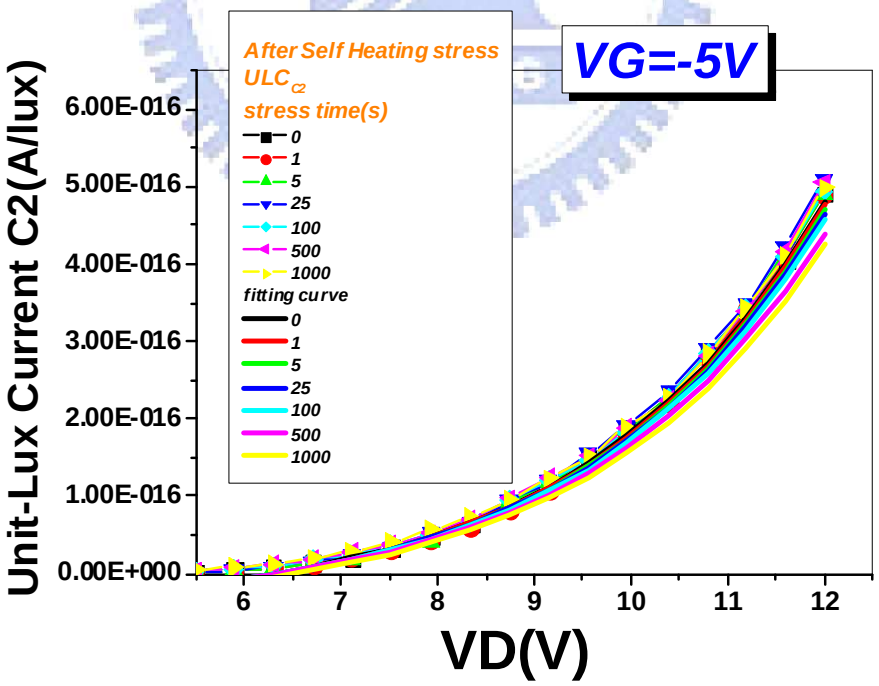

Fig. 3-11(b) The variation of ULC_{C2} versus VD at different S.H stress times.

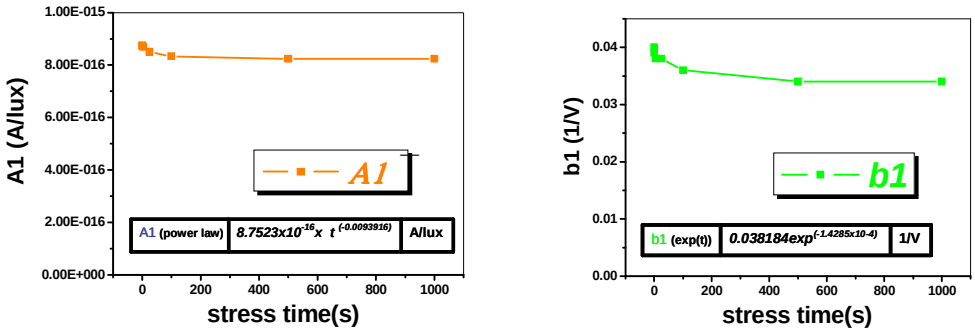

(a) (b)

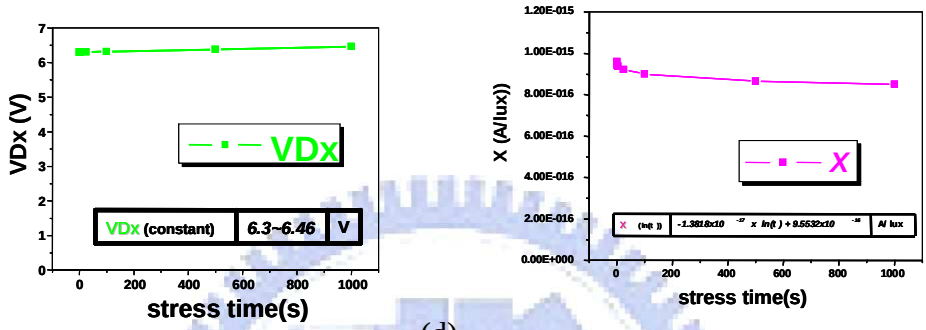

(c) (d)

Fig. 3-12(a) The variation of ULC_{C1} fitting factors (a) A1 (b) b1 (c)VDx (d) X versus VD at different S.H stress times.

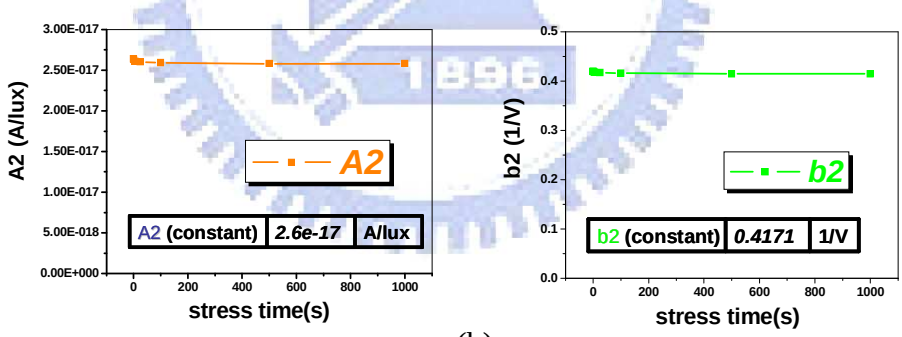

(a) (b)

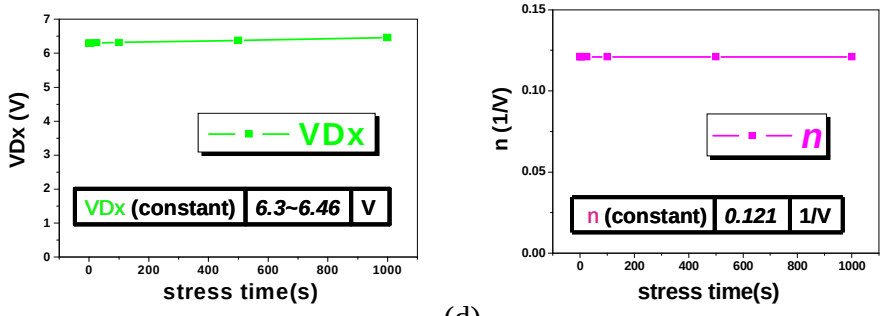

(c) (d)

Fig. 3-12(b) The variation of ULC_{C2} fitting factors (a) A2 (b) b2 (c)VDx (d) X versus VD at different S.H stress times.

3.3 Comparison and Discussion the Mechanism of Unit-Lux Current

Base on the results described 3-1 and 3-2, in this section, we try to propose the model to explain the effect of different defect states in the energy gap on photo leakage current of ULC_{C1} and ULC_{C2}.

Fig. 3-13 illustrates the model of both parameter *A1* and *b1* of ULC_{C1} (small VD) for unstressed devices. Wd indicates the length of depletion region at the drain electrode side where electron-hole pairs can be generated under illumination in the poly-Si film. Let's take a look at the part of the parameter *b1* first. As mentioned in 3-1-4, we know that the parameter *b1* is drain bias dependent on the amount of carriers generated per unit depletion area, wherein a sliced depletion area △X in diagram (a) is enlarged and shown in diagram (b). In this figure, we list several paths of carriers that will probably affect the parameter *b1*. First, the path (a) is band-to-band transition of carrier. It may overcome large energy gap, so the path (a) generally requires short wavelength light. The second path (b) is the carrier photo-excited from the trap near the valence band. Then, the third path (c) is carrier thermal-excited from the traps. In previous report, the behavior of ULC_{C1} (VD<6.3V) is explained by thermionic emission [7]. Thus, we infer that the path (c) is strongly correspond to ULC_{C1}. Additionally, the path (d) is dominated by field (or tunneling) that carriers excited from traps. Last, the path (e) is the electron-hole pair recombined through the trap. In the following, we will go through the above cases to propose the model for the behavior of *b1* after DC stress.

The main defects that H.C stress produces are tail states. Tail states locate close to either conduction band or valance band. Therefore, when the LTPS TFT devices after H.C stress are under optical illumination, we infer that path (a), (b) and (c) will

increase. So we are able to know that the parameter *b1* rises with stress times as shown in Fig. 3-6(a). In order to confirm the assumption, we have done another experiment to investigate the variation of the photo leakage current with respect to wavelength of light. Fig. 3-15(a) shows the photo leakage current before stress and after H.C stress (1000 sec) at VD=0.6V, VG=-5V. It is observed that the carrier can be excited from the trap by long wavelength light. It is attributed to the increase of tail states. Subsequently, we can find that the photo leakage current increases after H.C stress in this figure regardless of the wavelength.

On the other hand, the main defects that S.H stress produces are deep states. Deep states locate closely to the mid-gap. Therefore, when the LTPS TFT devices after S.H stress are under optical illumination, we infer that the path (e) will have a massive increase. Even though carriers might also be excited by the extra defects such as the path (a), (b) and (c), but we can find that the parameter *b1* reduces with stress times when these effects of paths are combined as shown in Fig. 3-12(a). We also have done the experiment to investigate the variation of the photo leakage current with respect to wavelength of light. Fig. 3-15 (b) shows the photo leakage current before stress and after S.H stress (1000 sec) at VD=0.6V, VG=-5V. We can observe that the photo leakage current reduces after S.H stress regardless of the wavelength.

Later on, let's turn to discuss parameter *A1*. We know that the parameter *A1* might be closer related to the factor which can influence the effective mobility in section 3-1-4. Thus, we also try to go through several possible paths of the carriers in the diagram (a) to discuss which will affect the parameter *A1*. First, the path (x) is the moving of carrier in the conduction band. It corresponds to the scattering (lattice scattering and coulomb scattering) and the mechanism of scattering are dependent on temperature. Thus, we will have a further discussion in the chapter 4. The second path (y) is that the carriers are captured by the shallow trap, and then re-excited to the band.

Above paths may delay the effective mobility.

While the tail state increases after H.C stress, we infer that the path (y) is relatively increasing. So we can obtain that the parameter *A1* decreases with stress times as shown in Fig. 3-6(a). On the other hand, when the deep state increases after S.H stress, we infer that the path (e) increasingly happens as well, but this path may not affect the carrier velocity. A few of tail states are generated after S.H stress in energy gap. There is still an opportunity that path (y) will happen. Therefore, we can also obtain that the parameter *A1* decreases with stress times as shown in Fig. 3-12(a).

Summing up these effects, ULC_{C1} increase with rise in H.C stress time and decrease with rise in S.H stress time as shown in Fig. 3-5(a) and Fig. 3-11(a).

Fig. 3-14 illustrates the model of the parameter *A2* and *b2* of ULC_{C2} (large VD) for unstressed devices. Let's take a look at the part of the parameter *b1* first. We know that the depletion region for large VD is full of the LDD region. Therefore, the increase of drain voltage will increase the electric field within the limited LDD length pinched by the n+ region. Such being the case, the parameter *b2* is related to the electric field. In Fig. 3-14(b), we also proposed probably paths of carriers that will affect the parameter *b2*. The path (d) is the carrier excited from the trap by field (or tunneling) same as that in Fig. 3-13(b). We know that the behavior of ULC_{C2} (VD>6.3V) is explained by field emission or tunneling [8]. Thus, we infer that the path (d) may correspond to ULC_{C2}. In addition, the path (e) is the same as that in Fig. 3-13(b). If the tail states increases in the energy gap, and then the probability of the path (d) will also increases. Therefore, we can find that the parameter *b2* also rises with H.C stress times increasing as shown in Fig. 3-6(b). On the other hand, if the deep states increases in the energy gap, the fact that the path (e) will occur. Despite of this, we still infer the probability will reduce, because the velocity of carriers is enhanced by the electric field increases, resulting in the probability of recombination

decrease. Thus, we can obtain that the parameter *b2* makes no big change after S.H stress as shown in Fig, 3-12(b).

Then, let's turn to discuss parameter *A2*. We infer that the parameter *A2* might be closer related to the effective mobility in section 3-1-4. Now, we try to go through several possible paths of the carriers in Fig. 3-14(a) to discuss which will affect the parameter *A2*. What is worth mentioning is that the paths (d') may delay the effective mobility. Compare to the path (d). The path (d') is considered that the carrier does not always excite directly from the trap to band. It has the tunneling possibility that the carriers may be hindered by the nearby tail state. Then, we further discuss the changing trend of the parameter A2 with different defect states. While the tail states increases after H.C stress carriers move through the path (d') may occurs. Therefore, we can observe that the parameter *A2* decreases with stress time as shown in Fig. 3-6(b). On the other hand, when the deep states increases after S.H stress, the path (e) will occur. Nevertheless, the path (y) may happen due to a few of tail states generated after S.H stress. Moreover, the velocity of carriers is enhanced by the electric field increases similarly, thus, we can find that the parameter *A2* decreases slightly with S.H stress times as shown in Fig. 3-12(b).

Synthesizes above effects of the parameter *A2* and *b2*, we can observe the results for ULC_{C2} as shown in Fig. 3-5(b) and Fig. 3-11(b). The photo leakage current decreases with the rise in H.C stress time and the photo leakage current makes no big change with rise in S.H stress time. We have done the experiment to investigate the variation of the photo leakage current with respect to wavelength of light similarly. Fig. 3-16 shows the photo leakage current on ULC_{C2} at VD=10V, VG=-5V that we subtract ULC_{C1} (VD=10V, VG=-5V) from the total ULC (VD=10V, VG=-5V). As show in Fig. 3-16(a), we can find the photo leakage current on ULC_{C2} is decreased after H.C stress. On the other hand, the photo leakage current on ULC_{C2} is also

decreased slightly after S.H stress.

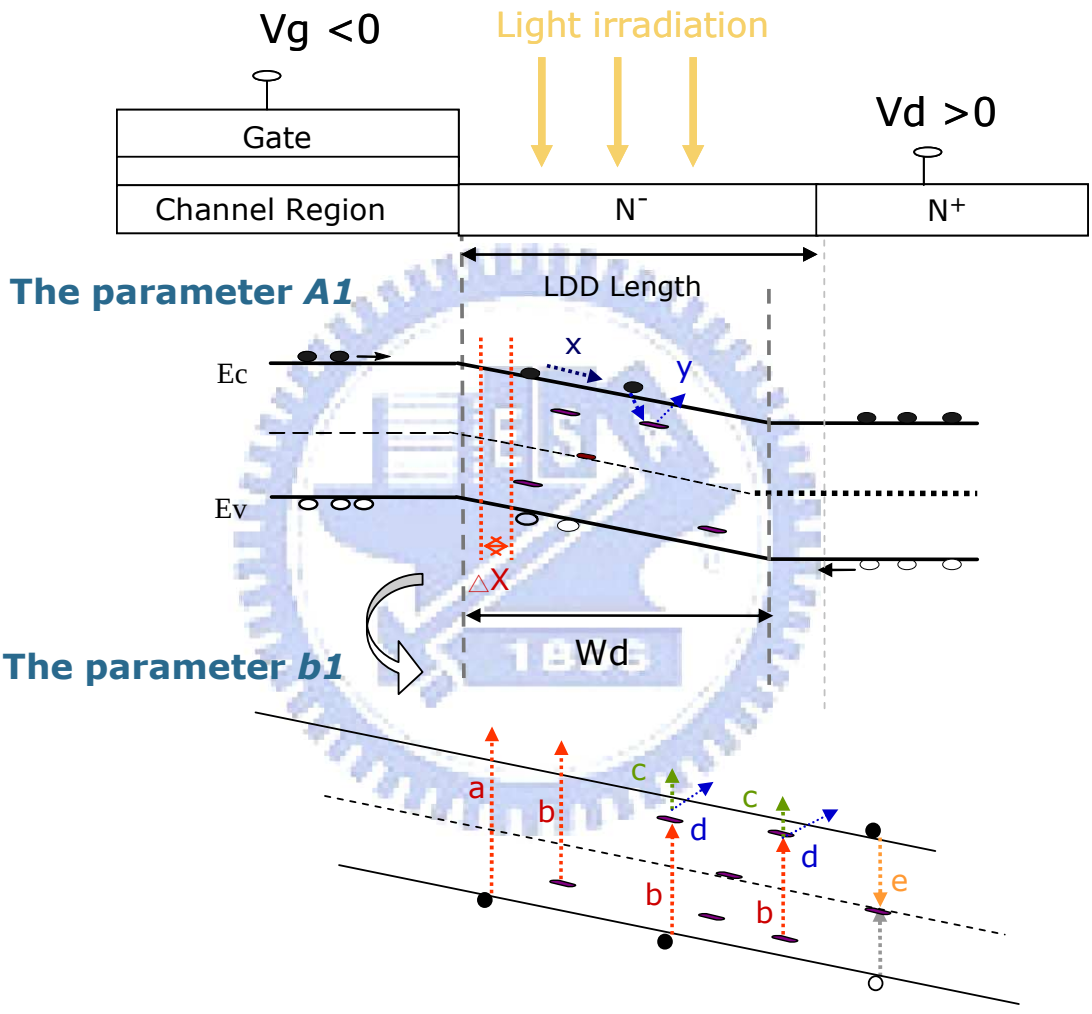

Fig. 3-13 Propose the model of the parameter *A1* and *b1* on $ULC_{C1.}$

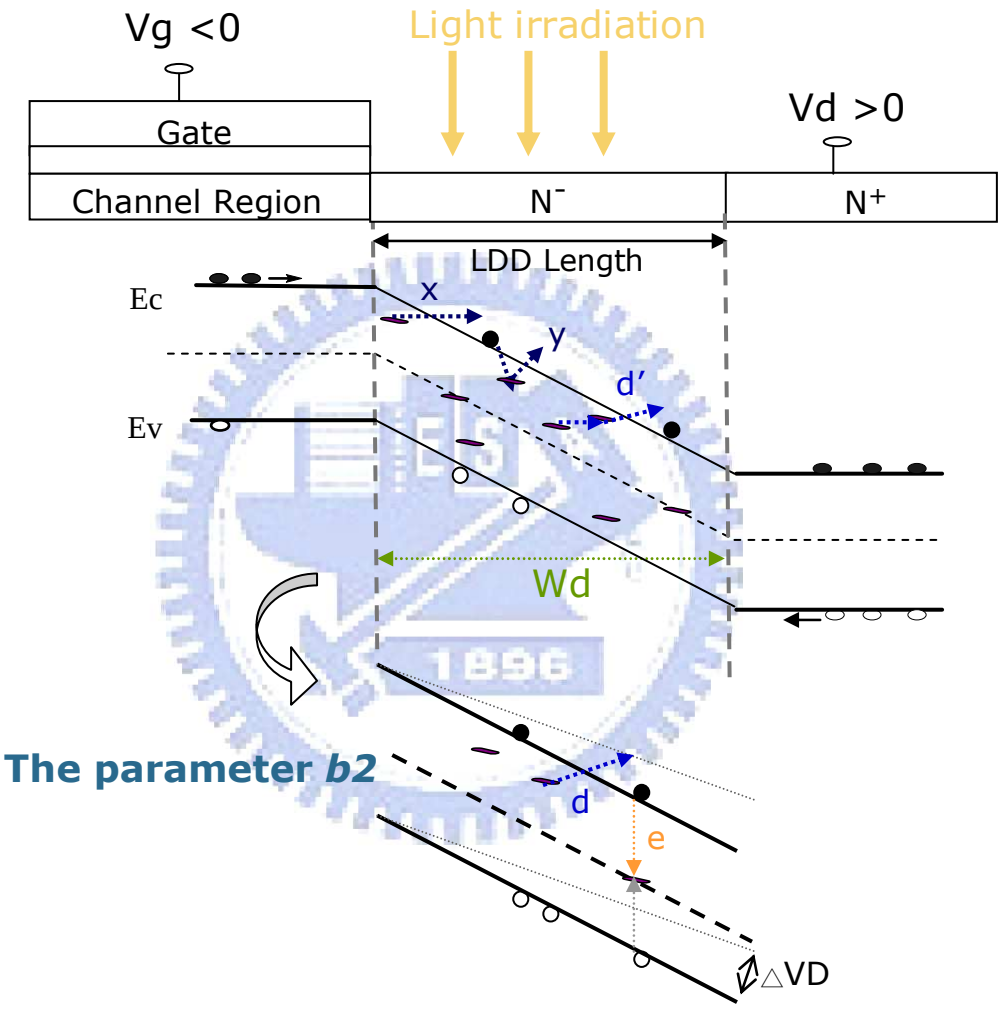

Fig. 3-14 Propose the model of the parameter *A2* and *b2* on $ULC_{C2.}$

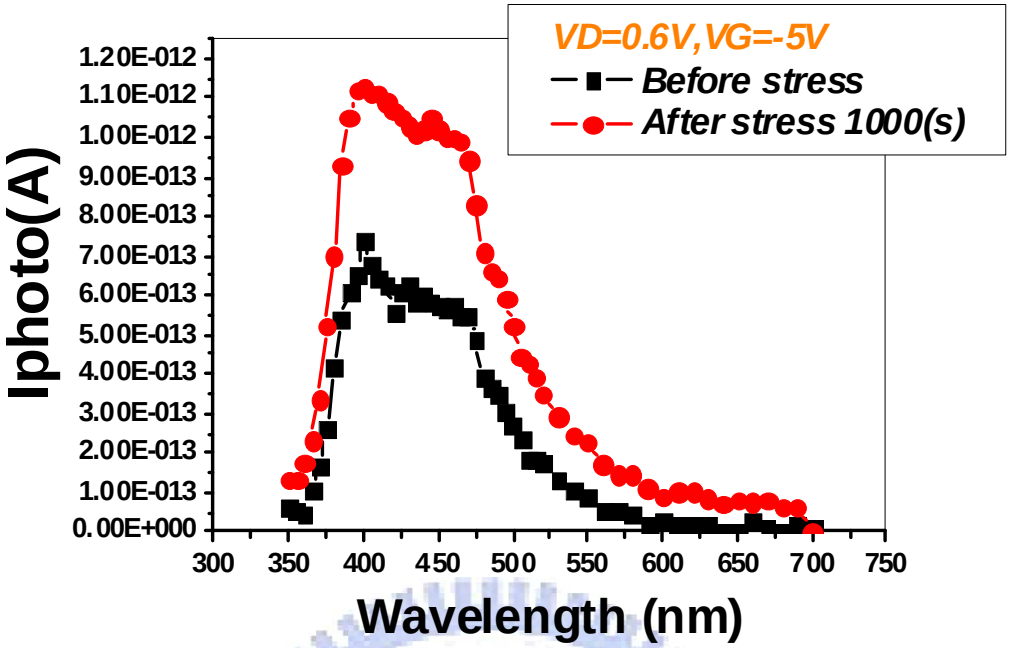

Fig. 3-15(a) The photo leakage current with different wavelength before and after H.C stress at (VD,VG)=(0.6V,-5V)

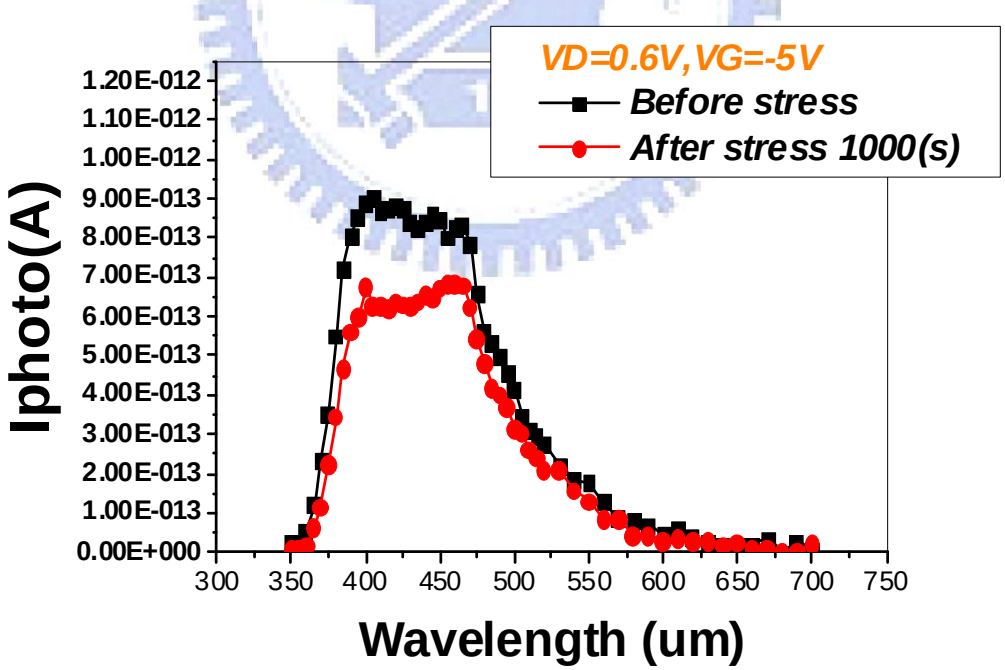

Fig. 3-15(b) The photo leakage current with different wavelength before and after S.H stress at (VD,VG)=(0.6V,-5V)

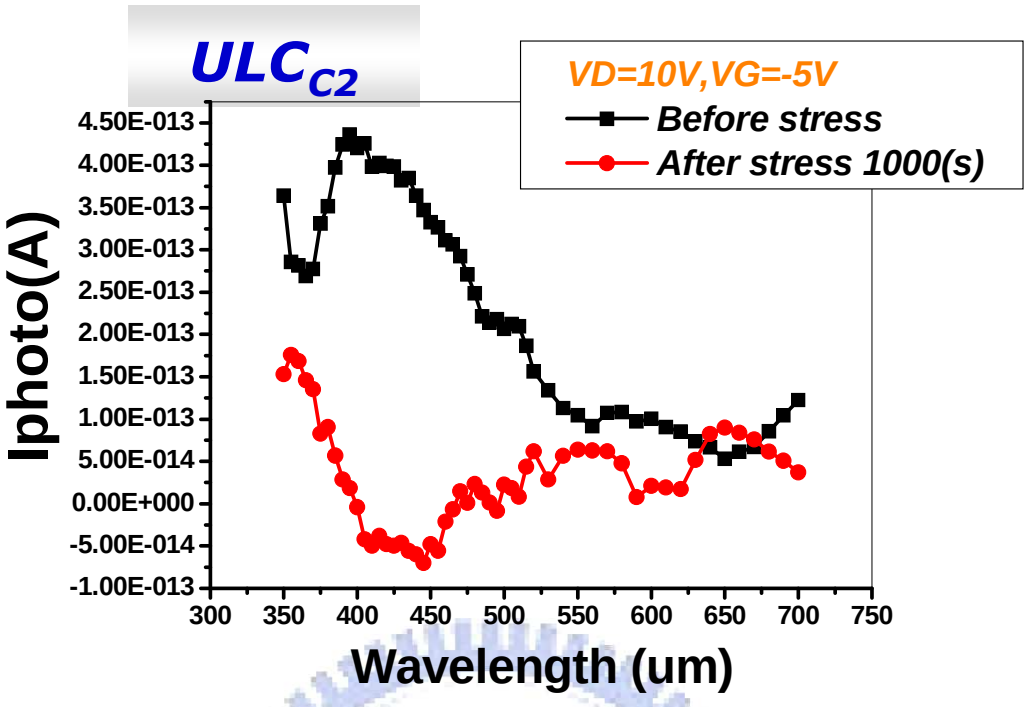

Fig. 3-16(a) The photo leakage current with different wavelength before and after H.C stress at (VD,VG)=(10V,-5V)

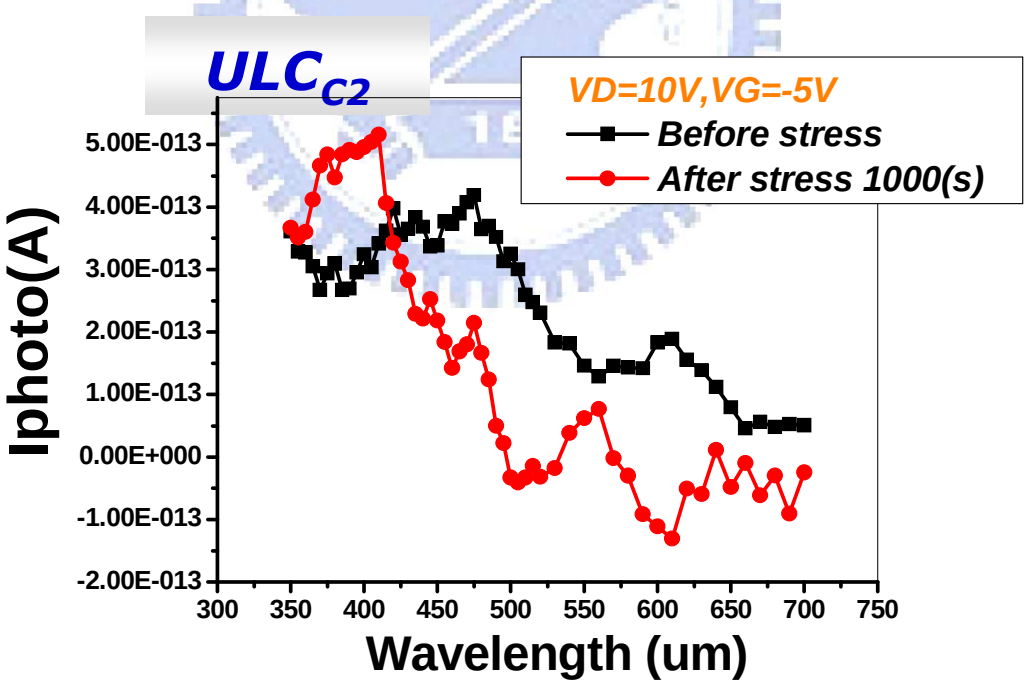

Fig. 3-16(b) The photo leakage current with different wavelength before and after S.H stress at (VD,VG)=(10V,-5V)

Chapter4

Effects of Temperature

4.1 Unstressed

4.1.1 Analysis Unit-Lux Current

In order to verify the mechanism and the physical significance of *A1* and *b1*, we designed the experiment for increasing temperature in an attempt to analyze the variation of ULC. The following Table4-1 lists this experiment systematically.

First of all, we must confirm that the relationship between Iphoto and illumination intensity at high temperatures is still linear. Thus the extraction of ULC can still make sense. Fig. 4-1 shows how the temperature influence on photo leakage current under a certain bias condition where (VD, VG) = (10V, -5V). Photo leakage current was measured under 25, 40 and 60 Celsius degree. It increases with temperature.

Fig. 4-2 shows drain bias dependence of ULC at different temperatures. It reveals that ULC rises with the increase in temperature. Hence, we investigate individual change for ULC_{C1} and ULC_{C2} in detail. Fig. 4-3(a) shows the variation of ULC_{C1} at different temperatures versus drain bias at VG=-5V. It also appears that the ULC_{C1} is lifted up with the rise in temperature. On the other hand, the ULC_{C2} has no correlation with temperature. The result is shown in Fig. 4-3(b).

4.1.2 Variation of Fitting Factors

Fig. 4-4 shows the change tendency of the parameters in associate with the empirical formula fitting ULC_{C1}. We can see *A1* decreases with rise in temperature. On the other hand, the parameter *b1* increases with rise in the temperature. *VDx*

maintains at 6.3V, and the parameter *X* increase with temperature. We will discuss in more detail by comparing the cases of unstressed as well as those of hot carrier stress and self heating stress in section 4-4.

Temperature	25, 40, 60(℃)

EXPERIMENT	Gate Bias (V)	Drain Bias (V)	Illumination Intensity (lux)
VG step VD sweep	-5	0.6 ~ 12 Interval: 0.4071V	0 1566 5940 14486 26460 51300
	-7.5		
	-10		
VD step VG sweep	-2~ -10 Interval:0.4V	0.6	
		5.3	
		10	

Table 4-1 Experiment conditions for temperature and VD, VG effects on photo leakage.

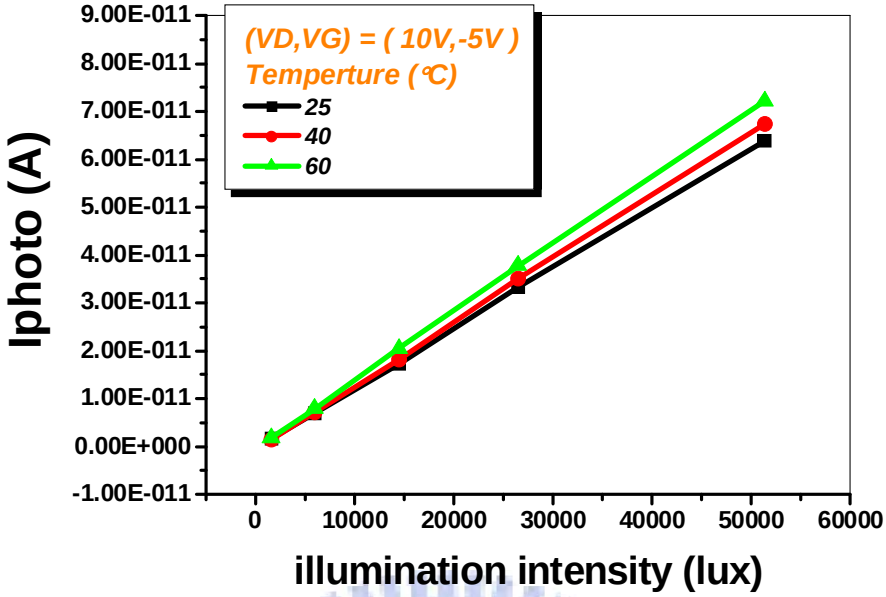

Fig. 4-1 The temperature effect on photo leakage current under a certain bias condition (VD, VG) = (10V, -5V)

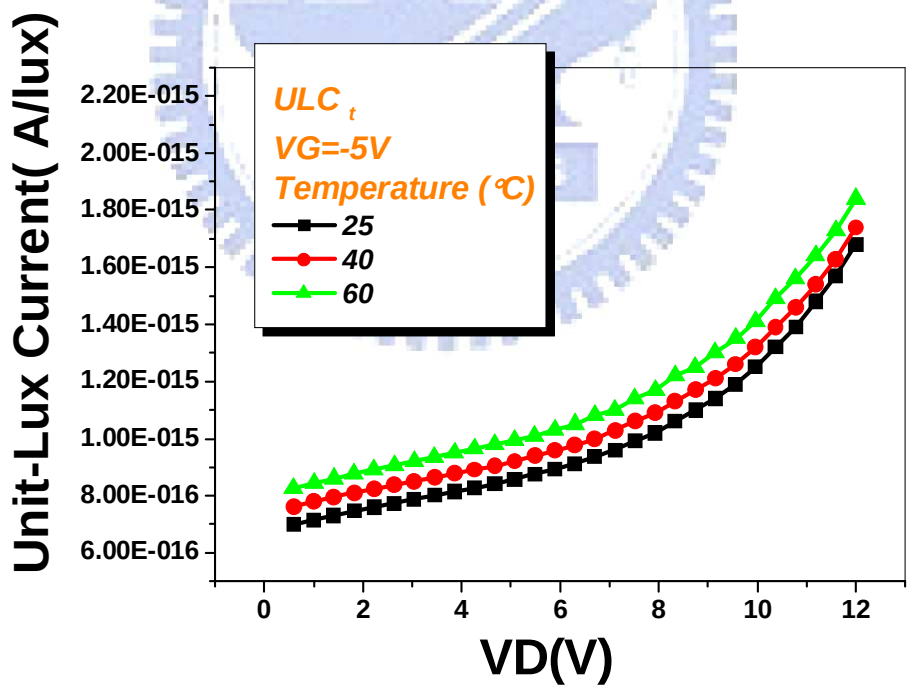

Fig. 4-2 Drain bias dependence of Unit-Lux Current at different temperature

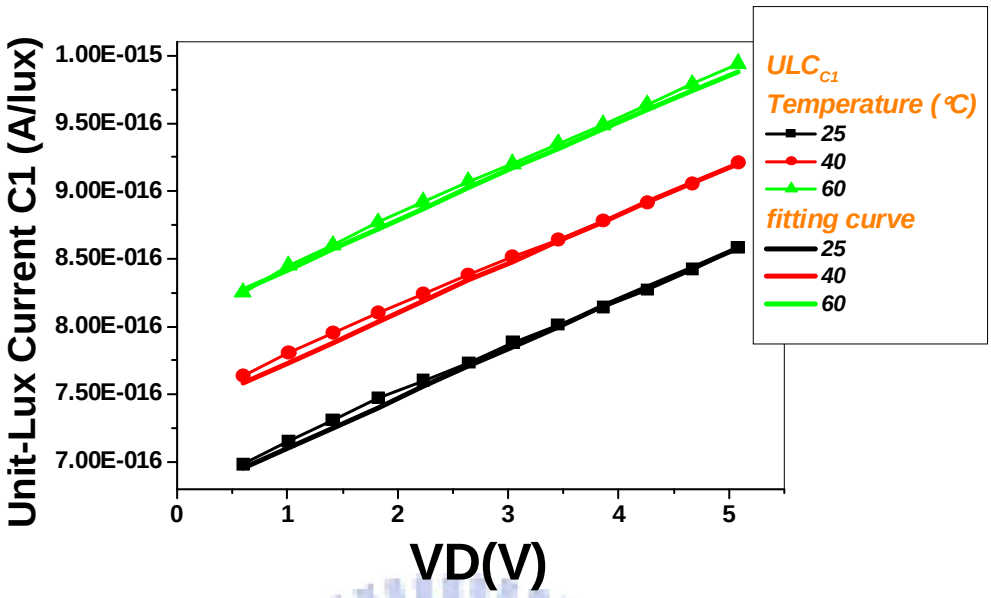

Fig. 4-3(a) The variation of ULC_{C1} at different temperature versus drain bias in VG=-5V.

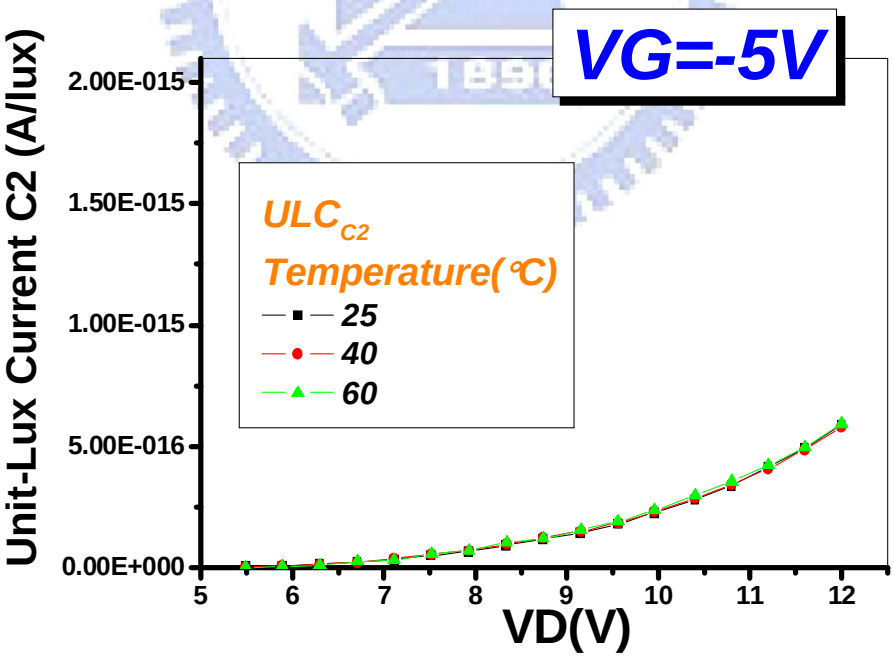

Fig. 4-3(b) The variation of ULC_{C2} at different temperature versus drain bias in VG=-5V.

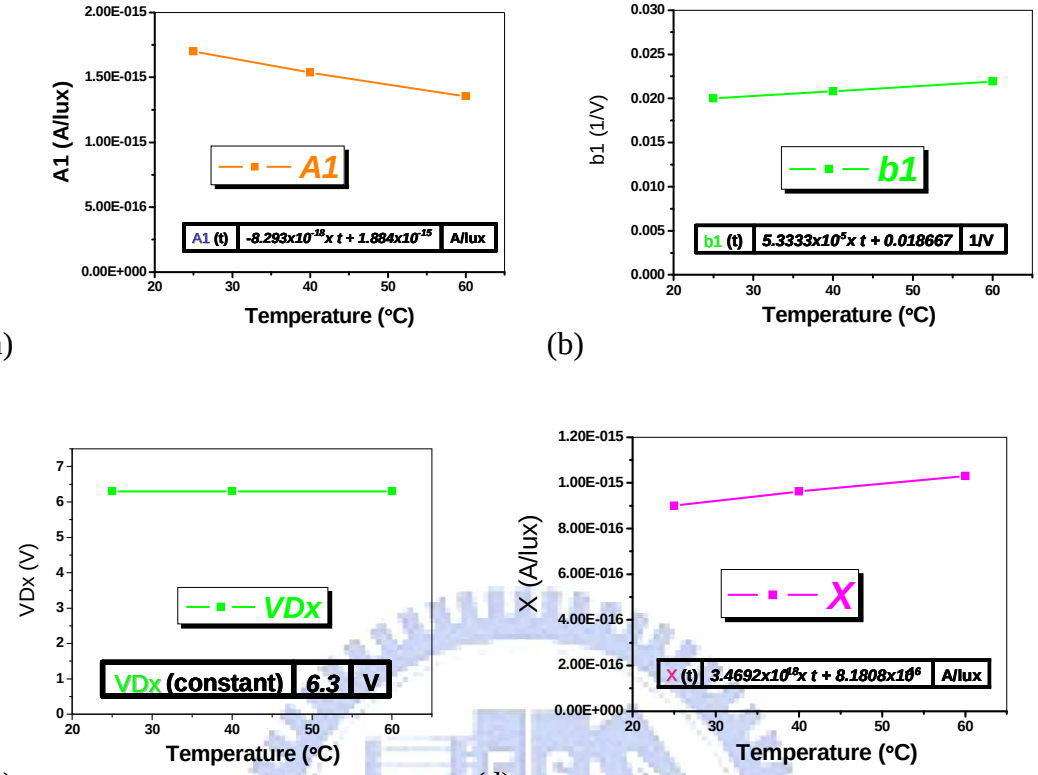

(a) (b)

(c) (d)

Fig. 4-4 The variation of ULC_{C1} fitting factors (a) A1 (b) b1 (c) VDx (d) X versus VD at different temperature.

4.2 Case of Hot Carrier Stress

4.2.1 Analysis Unit-Lux Current

Again, we need to confirm that the relationship between Iphoto and illumination intensity after hot carrier stress with temperature is still linear. Fig. 4-5 shows how the temperature influence on photo leakage current of the TFT after H.C stress under the bias condition where (VD, VG) = (10V, -5V). Fig. 4-6 shows drain bias dependence of ULC at different temperature. It also reveals that ULC rises with the increase in temperature. Hence, we investigate individual change for ULC_{C1} and ULC_{C2} in detail. Fig. 4-7(a) shows the variation of ULC_{C1} at different temperature versus drain bias in VG=-5V. It also appears that the ULC_{C1} is lifted up with the rise in temperature. On

the other hand, the ULC_{C2} remains to be independent of temperature. The result is shown in Fig. 4-7(b).

4.2.2 Variation of Fitting Factors

Fig. 4-8 shows that the change tendency of the parameters that we use the new empirical formula fitting ULC_{C1}. We can see *A1* decreases with rise in temperature. On the other hand, the parameter *b1* increase with rise in the temperature. *VDx* maintains in 6.3V, and the parameter *X* increase with temperature.

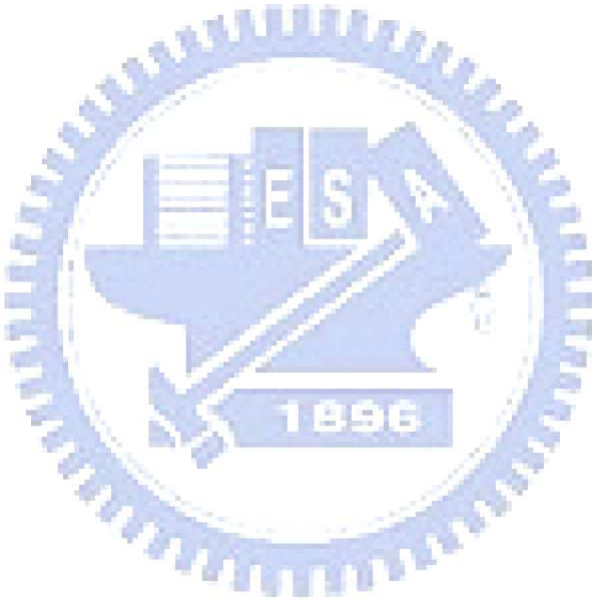

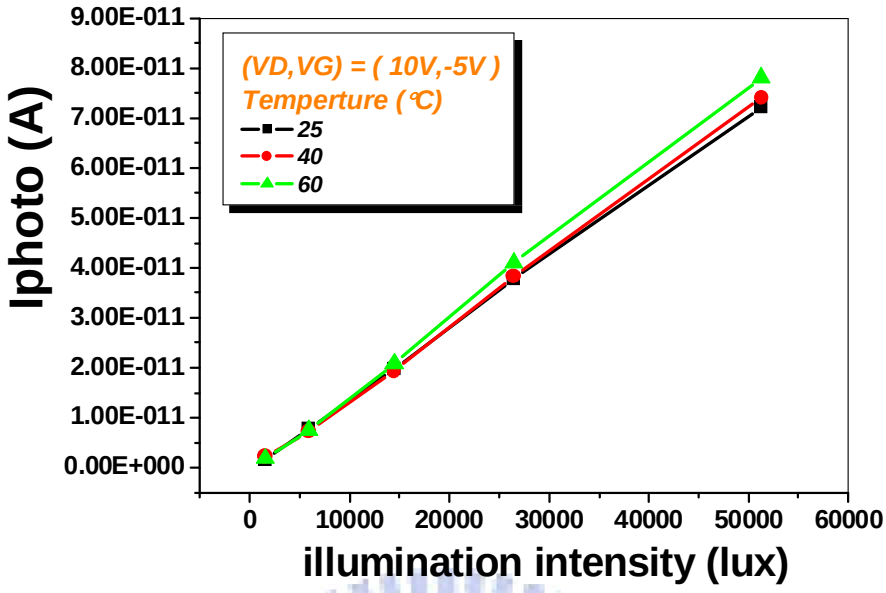

Fig. 4-5 The temperature effect on photo leakage current after hot carrier stress under a certain bias condition (VD, VG) = (10V, -5V)

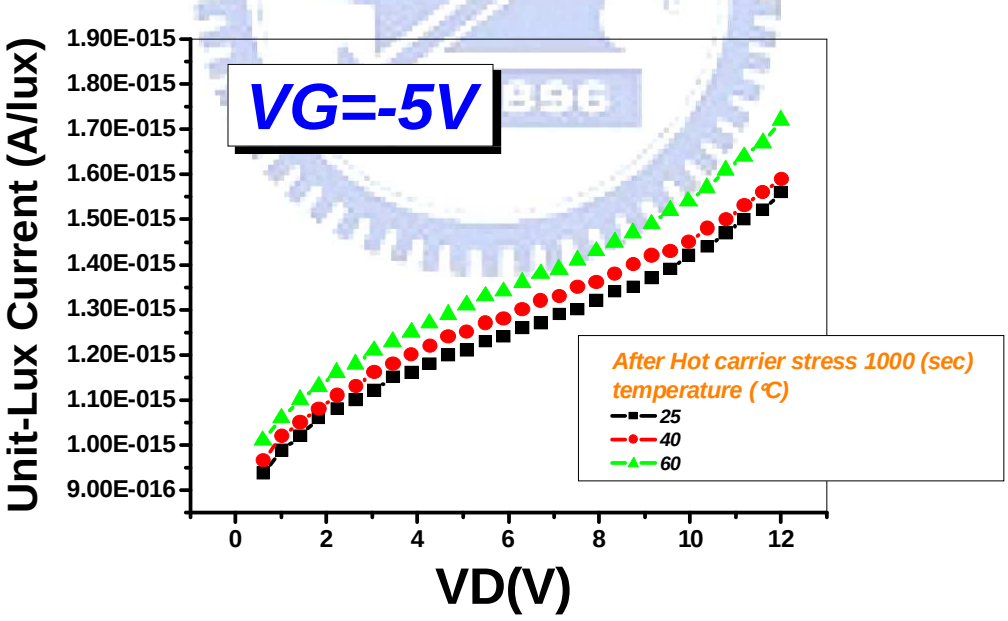

Fig. 4-6 Drain bias dependence of Unit-Lux Current after H.C stress at different temperature

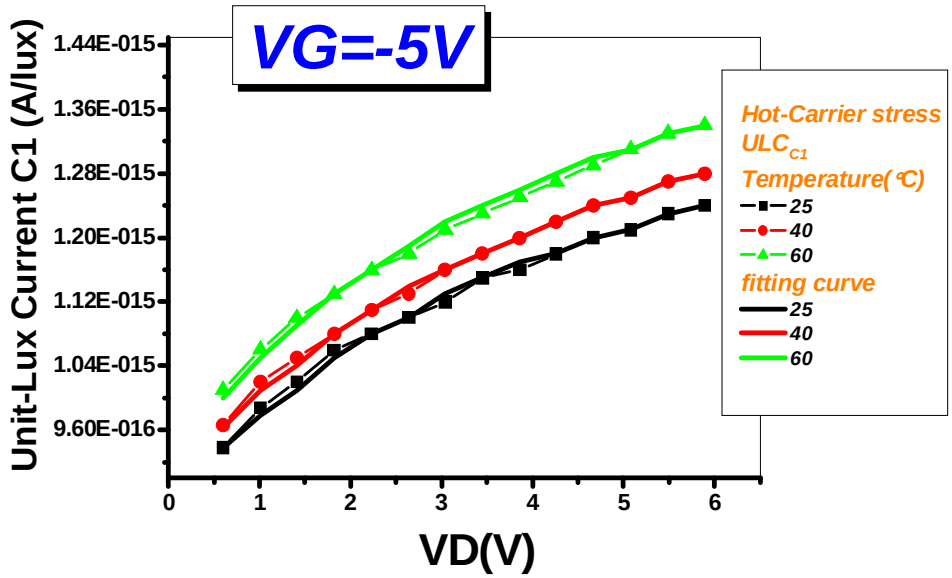

Fig. 4-7(a) The variation of ULC_{C1} after H.C stress at different temperature versus drain bias in VG=-5V.

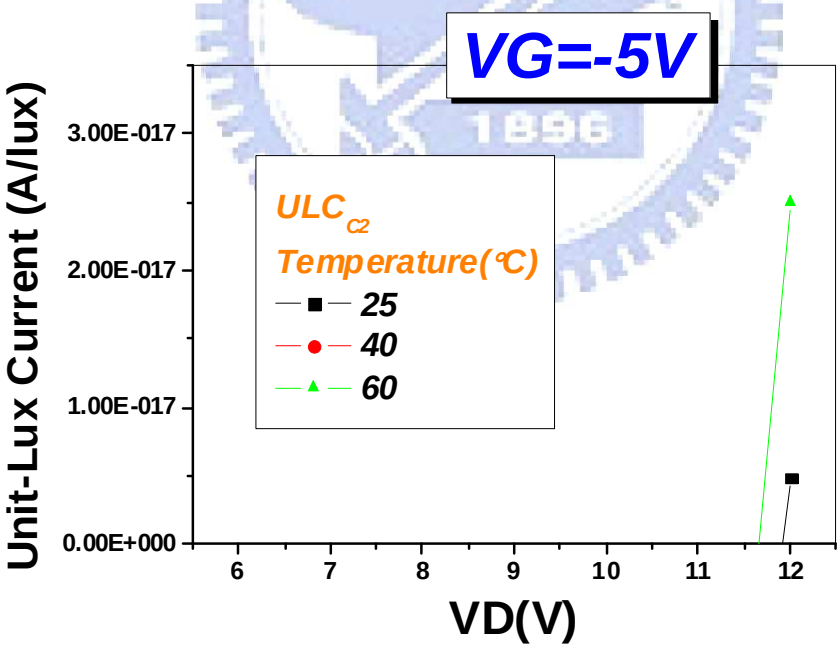

Fig. 4-7(b) The variation of ULC_{C1} after H.C stress at different temperature versus drain bias in VG=-5V

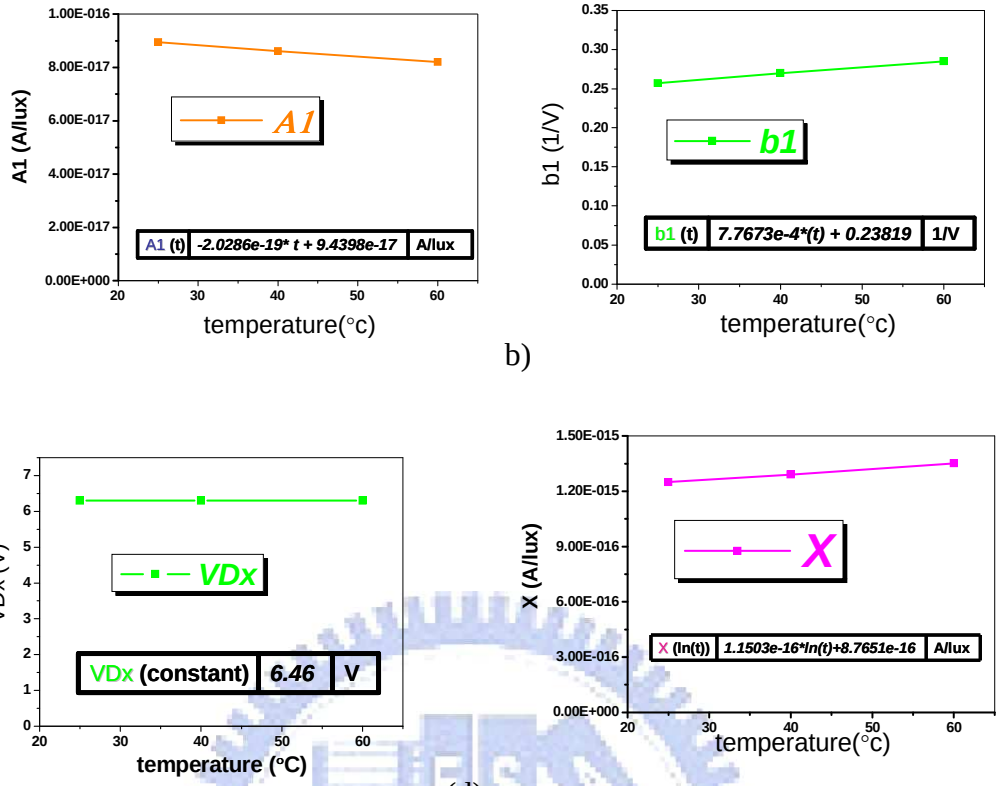

(a) b) (c) (d)

Fig. 4-8 The variation of ULC_{C1} fitting factors (a) A1 (b) b1 (c) VDx (d) X versus VD after H.C stress at different temperature.

4.3 Case of Self Heating Stress

4.3.1 Analysis Unit-Lux Current

Similarly, we need to confirm that the relationship between Iphoto and illumination intensity after S.H stress with temperature is still linear. Fig. 4-9 shows how the temperature influence on photo leakage current after S.H stress under a certain bias condition where (VD, VG) = (10V, -5V). Drain bias dependence of ULC at different temperature as shown in Fig. 4-10. It reveals that ULC rises with the increase in temperature. Hence, we investigate individual change for ULC_{C1} and ULC_{C2} in detail. Fig. 4-11(a) shows the variation of ULC_{C1} at different temperature versus drain bias in VG=-5V. It also appears that the ULC_{C1} is lifted up with the rise in temperature. On the other hand, the ULC_{C2} remains to be independent of temperature similarly. The result is shown in Fig. 4-11(b).

4.3.2 Variation of Fitting Factors

Fig. 4-8 shows that the change tendency of the parameters that we use the new empirical formula fitting ULC_{C1}. We can see *A1* decreases with rise in temperature. On the other hand, the parameter *b1* increase with rise in the temperature. *VDx* maintains in 6.3V, and the parameter *X* increase with temperature.

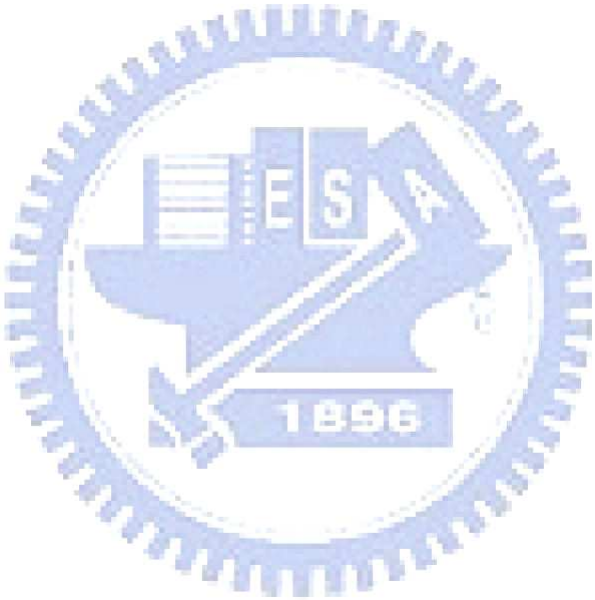

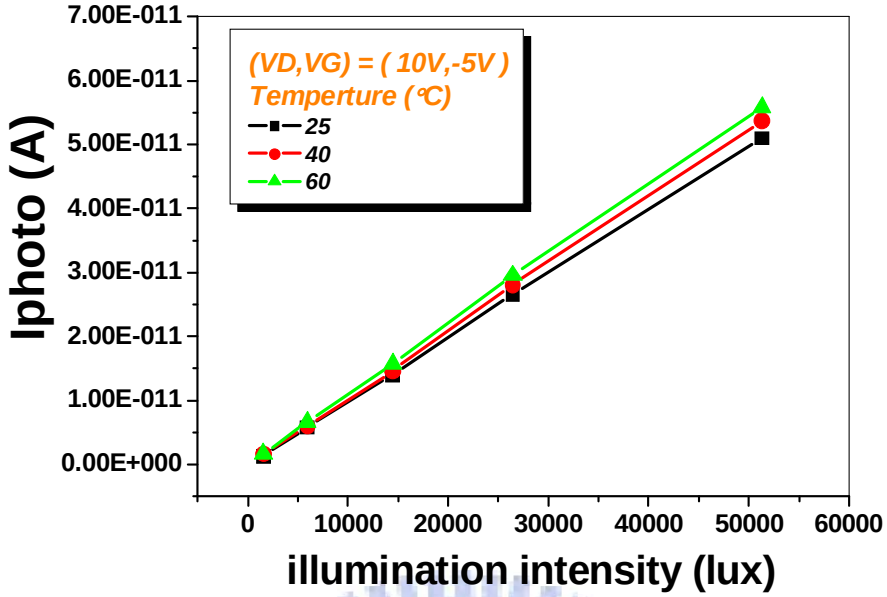

Fig. 4-9 The temperature effect on photo leakage current after self heating stress under a certain bias condition (VD, VG) = (10V, -5V)

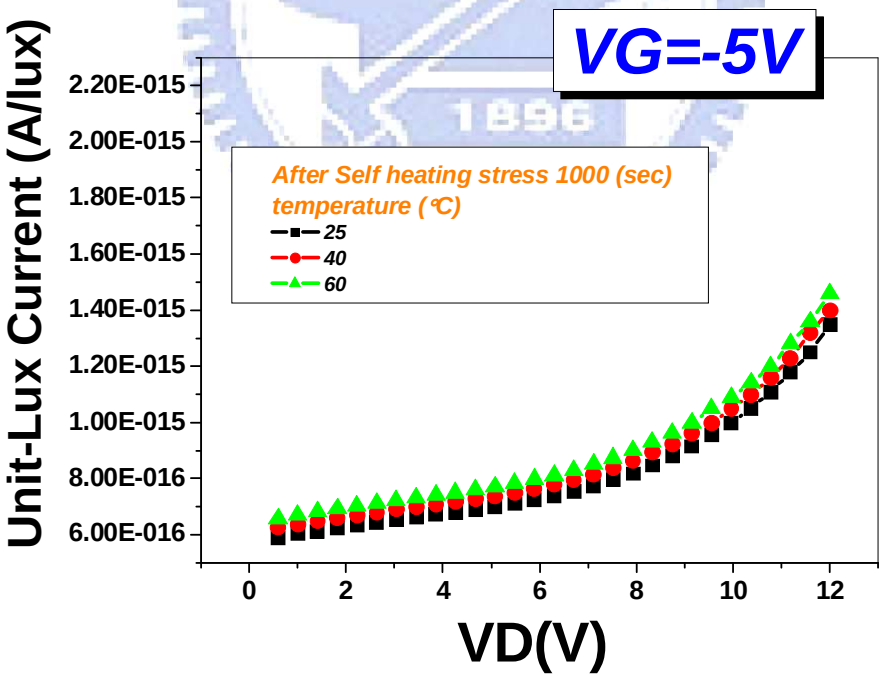

Fig. 4-10 Drain bias dependence of Unit-Lux Current after S.H stress at different temperature

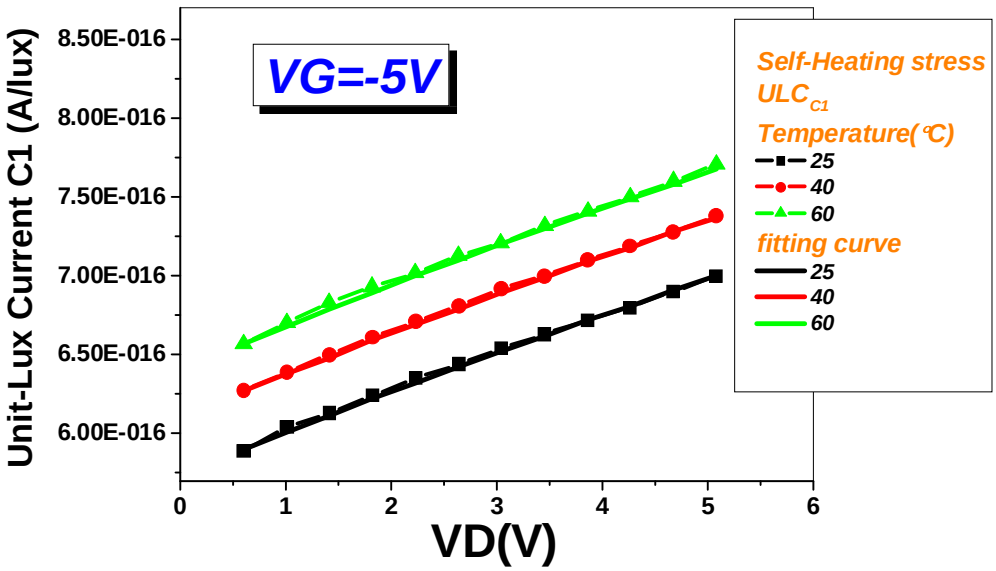

Fig. 4-11(a) The variation of ULC_{C1} after S.H stress at different temperature versus drain bias in VG=-5V.

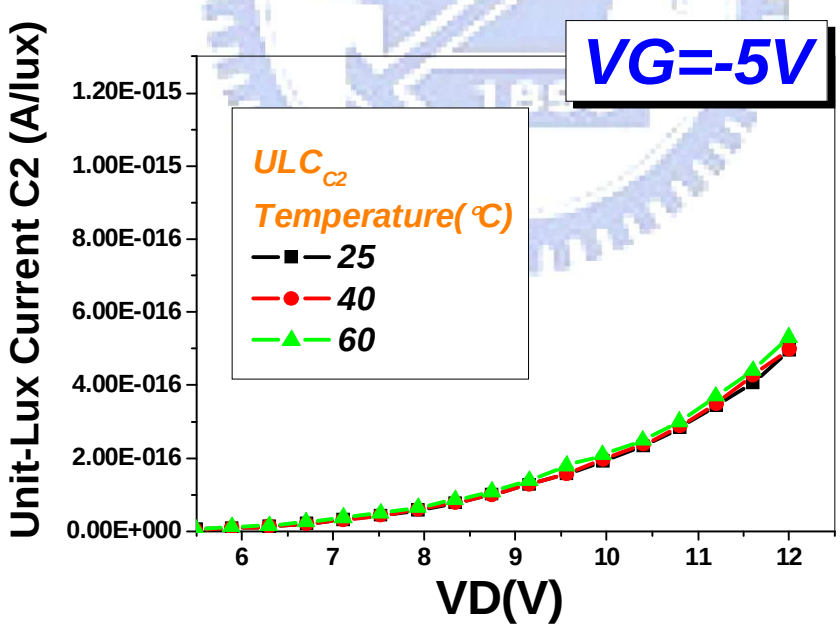

Fig. 4-11(b) The variation of ULC_{C2} after S.H stress at different temperature versus drain bias in VG=-5V.

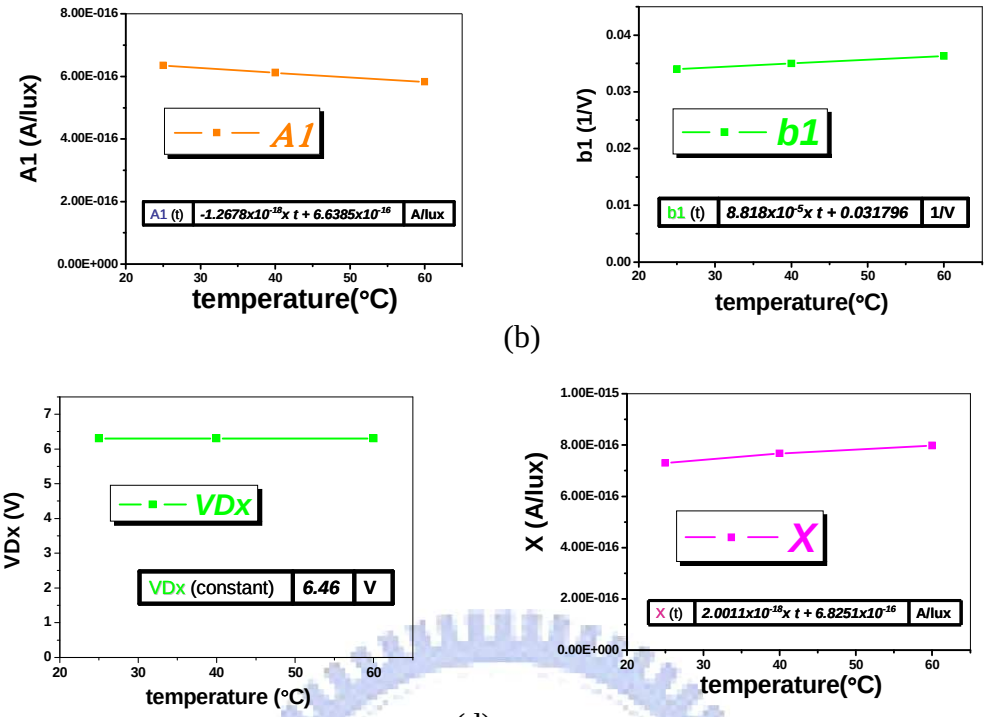

(a) (b)

(c) (d)

Fig. 4-12 The variation of ULC_{C1} fitting factors (a) A1 (b) b1 (c) VDx (d) X versus VD after S.H stress at different temperature.

4.4 Summary

We already know the change in the parameters of the new empirical formula fitting ULC_{C1} for the conditions of unstressed, H.C stress and S.H stress. As we mentioned in the previous discussion, the parameter *A1* may relate to the effective mobility. Fig. 4-13 shows the variation of relative *A1* normalized to the value at room temperature versus temperature for the cases of unstressed, H.C stress and S.H stress. We can see that the parameter *A1* of the unstressed device decreases more than those devices after H.C stress and S.H stress with respect to the rise in temperature. We conjectured that it is because the lattice scattering increases with the rise in temperature for the case of unstressed [9]. Hence, the effective mobility reduces more with the temperature. On the other hand, because many extra defects are created after H.C stress and S.H stress, the defect scattering (coulomb scattering) becomes more important. Since the defect scattering exhibits negative temperature dependent,

opposition to the lattice scattering, the temperature dependents on *A1* for the TFTs after H.C or S.H stress are less that for the unstressed one.

On the other hand, we surmise that the parameter *b1* may correspond with the number of carriers generated in per unit depletion area in section 3-3. Referring to Fig. 4-13(b), our supposition will be verified as follow. The number of carriers re-excited from the tail state in unit-area in depletion region increases with the rise in temperature, but decreases owing to the recombination by deep state. Therefore, the slope of *b1* for hot carrier stress is greater than that for the unstressed device, while the slope of *b1* for self heating stress is even smaller.

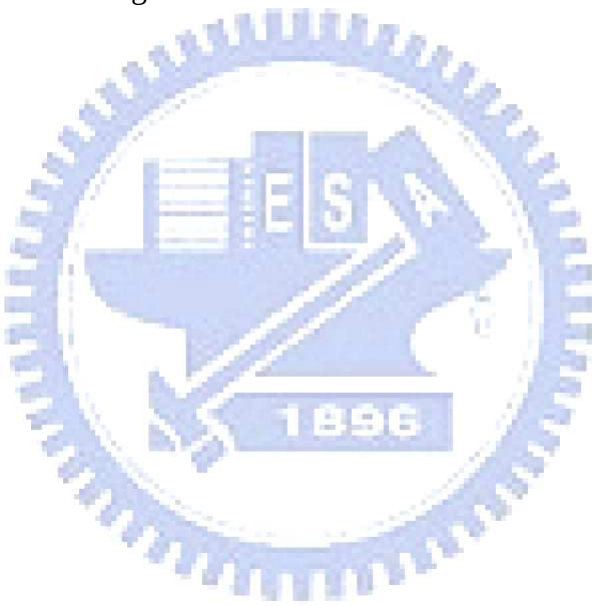

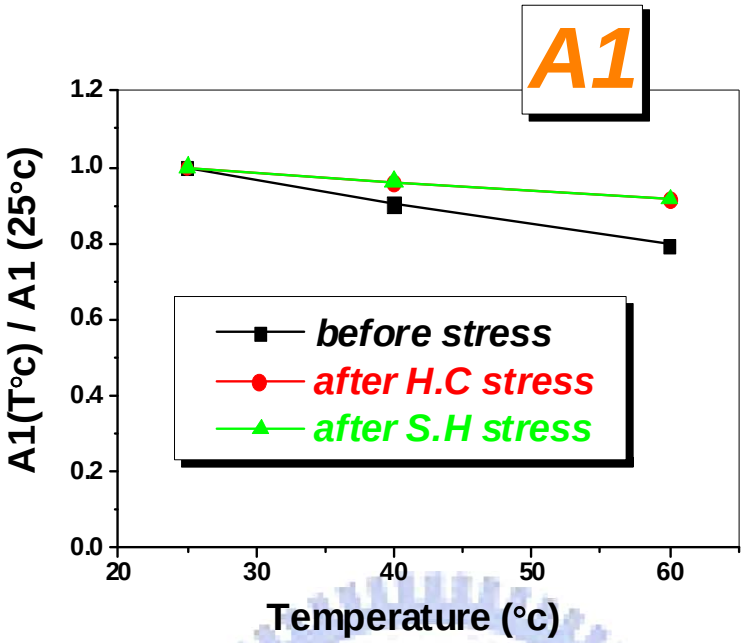

Fig. 4-13(a) The normalization of A1 versus temperature under the condition of unstressed, hot carrier stress and self heating stress.

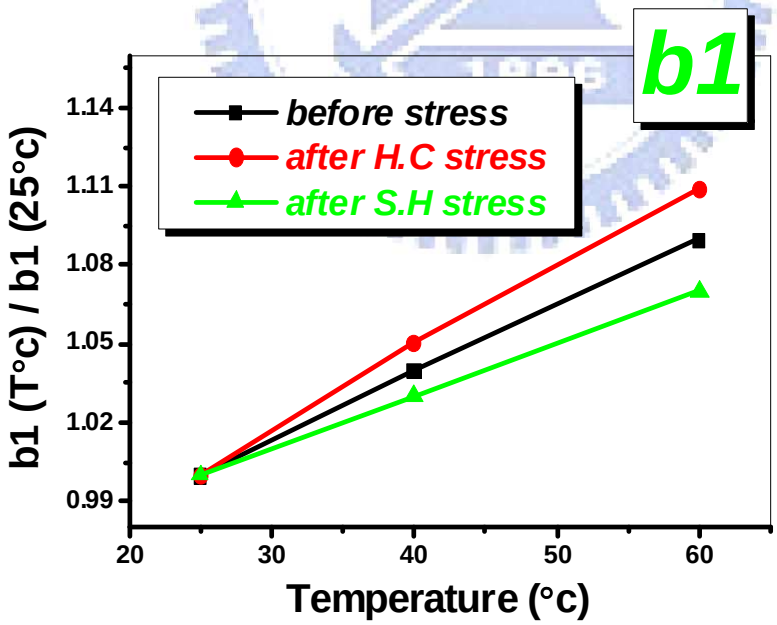

Fig. 4-13(b) The normalization of b1 versus temperature under the condition of unstressed, hot carrier stress and self heating stress.

Chapter5

Conclusions

In this thesis, first of all, we confirm that the photo leakage current occurs mainly on the drain side and focus on that region. We also revise the empirical formula for ULC to provide even more accurate description of the photo induced current under the presentation of defect states and temperature.

A ULC model for TFT is proposed to explain the illumination behaviors corresponding to the defects created after hot carrier stress and self heating stress. For low drain voltages (ULC_{C1}), hot carrier stress creates tail state defects that enhance photo leakage current by thermal or photo re-excitement, but self heating stress creates deep state defects that reduce photo leakage current by recombination. For high drain voltages (ULC_{C2}), because the carriers may be hindered by the nearby tail state in transport process, that will decrease the carrier mobility. Thus, the photo leakage current reduces after hot carrier stress. On the other hand, because the velocity of carrier is enhanced by electric field increases, so the probability of recombination is decreased. Therefore, the photo leakage current reduces slightly after self heating stress.

Appendix

In this experiment, the device we used were the conventional top-gate structure n-channel LTPS TFTs. The cross-section views of n-channel LTPS TFTs are shown in Figure below. The process flow of TFTs is described as follows: First, the buffer oxide and 50 nm thick a-Si:H films were deposited on glass substrates with plasma-enhanced chemical vapor deposition (PECVD). The samples were then put into the oven for dehydrogenation. The XeCl excimer laser of wavelength 308 nm and energy density of 400 mJ/cm^2 was used to recrystallize the a-Si:H film to poly-Si. After poly-Si active area definition, 65nm gate insulator was deposited with PECVD. Next, the metal gate was formed by sputter and then defined. The lightly doped drain (LDD) and the n+ source/drain doping were formed by PH3 implantation with dosage 2×10^{13} and 2×10^{15} cm^2 of PH_3, respectively. The LDD implantation was self-aligned and the n+ regions were defined with a separate mask. Then the interlayer of SiN_X was deposited. Subsequently, the rapid thermal annealing was conducted to activate the dopants. Meanwhile, the poly-Si film was hydrogenated. Finally, the contact holes formation and metallization were performed to complete the fabrication work. The channel width of TFTs is 20 μm and channel length is 5 μm, while the length of the LDD region is 2.5 μm.

The current-voltage characteristic of LTPS TFTs was measured by HP 4156A semiconductor parameter analyzer. We had focused our attention on the leakage current in the off-region under illumination. Photo leakage current was induced by a halogen lamp irradiation stream with several intensities through the objective of a microscope, and the light intensity was measured by a digital luminous flux meter.

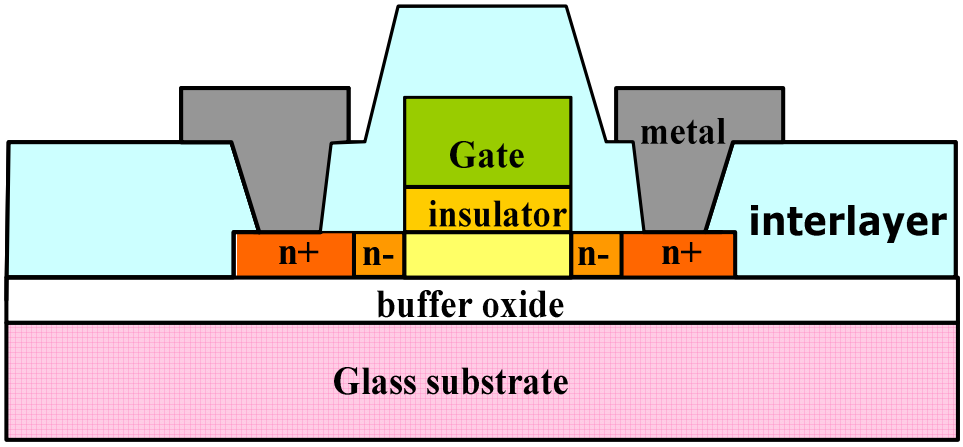

The cross-section views of n-channel LTPS TFTs with LDD structure

REFERENCE

[1]. Ya-Hsiang Tai, Yan-Fu Kuo, and Yun- Hsiang Lee, “Photosensitivity analysis of low-temperature poly-Si thin-film transistor based on Unit-Lux Current”, IEEE Trans. Electron Devices, Vol. 56, no. 1, pp. 50–56, January 2009.

[2]. Y. Nanno, K. Senda, H. Tsutsu, “Analysis of photocurrents in low-temperature polysilicon thin-film transistors and the use of simulation to design LDD devices”, Electronics and Communications in Japan, Part 2, Vol. 86, No. 11,2003

[3]. K. Kobayashi, and Y. Niwano, “Photo-Leakage Current of Poly-Si Thin Film Transistors with Offset and Lightly Doped Drain Structure”, Jpn. J. Appl. Phys., Vol. 38, pp. 5757-5761, 1999.

[4]. Y. Uraoka, T. Hatayama, T. Fuyuki, T. Kawamura and Y. Tsuchihashi, “Hot Carrier Effects in Low-Temperature Polysilicon Thin-Film Transistors”, Jpn. J. Appl. Phys., Vol. 40, pp. 2833-2836, 2006.

[5]. Ya-Hsiang Tai, Yan-Fu Kuo, and Yun- Hsiang Lee, ”Dependence of Photosensitive Effect on the Defects Created by DC Stress for LTPS TFTs”, Electron Devices Letter, IEEE Vol. 29, Issue 12, pp. 1322–1324, Dec. 2009.

[6]. S. Inoue, H. Ohshima and T. Shimoda, “Analysis of Degradation Phenomenon Caused by Self-Heating in Low-Temperature-Processed Polycrystalline Silicon Thin Film Transistors,” Jpn. J. Appl. Phys., Vol. 41 pp. 6313-6319, Nov 2002.

[7]. C. H. Kim, K.-S. Sohn, and J. Jang, “Temperature dependent leakage currents in polycrystalline silicon thin film transistors”, J. Appl. Phys.,vol. 81, no. 12, pp. 8084–8090, Jun. 1997.

[8]. G. Fortunato and P. Migliorato, “Determination of gap state density in polycrystalline silicon by field-effect conductance,” Appl. Phys. Lett., vol. 49, no.16, pp. 1025–1027, Oct. 1986.

[9]. A. Sehgal, T. Mangla, M. Gupta," Temperature dependence on electrical characteristics of short geometry poly-crystalline silicon thin film transistor", Solid-State Electron, vol. 49, pp. 301-309, 2005

[10]. K . R. Olasupo and M. K. Hatalis, "Leakage current mechanism in sub-micron polysilicon thin-film transistors," IEEE Trans. Electron Devices, Vol. 43, no. 8, pp. 1218–1223, Aug. 1996.

[11]. J. R. Ayres, S. D. Brotherton, I. R. Clarence and P. J. Dobson, "Photocurrents in poly-si TFTs," IEE Proc.-Circuits Devices Syst. ,Vol. 141, No.1, February 1994.

[12]. N. P. Papadopoulos, A. A. Hatzopoulos, D. K. Papakostas, C. A. Dimitriadis, and S. Siskos, "Modeling the impact of light on the performance of polycrystalline thin-film transistors at the sub-threshold region," Microelectronics Journal 37 (2006), 1313-1320.

[13]. C. H. Kim, K.-S. Sohn, J. Jang, "Temperature dependent leakage currents in polycrystalline silicon thin film transistors", Journal of Applied Physics, vol 81, no 12, p. 8084, Jun. 1997.

[14]. O. K. B. Lui, P. Migliorato, "New generation-recombination model for device simulation including the Poole-Frenkel effect and phonon-assisted tunnelling," Solid-State Electronics, vol 41, no 4, pp. 575-583, Apr. 1997.

[15]. F. Matsuki, K. Hashimoto, K. Sano, D. Yeates, J. R. Ayres, M. Edwards, and A. Steer, "Integrated ambient light sensor in LTPS AMLCDs," in Proc. Society for Information Display, 2007, pp. 290-293

[16]. H. Mori, K. Hata, T. Hashimoto, I-Wei Wu, Alan G. Lewis, M. Koyanagi, "Low-temperature operation of polycrystalline silicon thin-film transistors", Jpn. J. Appl. Phys., Vol. 30, pp. 3710-3714, 1991.

[17]. A. Valletta, L. Mariucci, and G. Fortunato, "Hot-carrier-induced degradation of LDD polysilicon TFTs", IEEE Trans. Electron Devices, Vol. 53, no. 1, pp.

50–56, January 2009.

[18]. W. J Wu, R. H. Yao, S. H. Li, Y. F. Hu, W. L. Deng, X. R. Zheng, “A compact model for polysilicon TFTs leakage current including the Poole-Frenkel effect,” IEEE Transactions on Electron Devices, vol 54, no 11, pp. 2975-2983, Nov 2007.

[19]. J. H. Chen, S. C. Wong, Y. H. Wang, “An analytic three-terminal band-to-band tunneling model on GIDL in MOSFET,” IEEE Trans. on Electron Devices, vol 48, no 7, pp. 1400-14053, Jul. 2001.

[20]. M.J. Siddiqui, S. Qureshi, “An empirical model for leakage current in poly-silicon thin film transistor”, Solid-State Electronics, vol. 44, pp. 2015-2019, 2000

[21]. M. D. Jacunski, M. S. Shur, A. A. Owusu, T. Ytterdal, M. Hack, Benjam´ın Iˇn´ıguez, “A short-channel DC SPICE model for polysilicon thin-film transistors including temperature effects”, IEEE Trans. on Electron Devices, vol 46, no 6, pp. 1146 - 1158, June. 1999.

[22]. Ya-Hsiang Tai, Shih-Che Huang, Chien-Wen Lin, and Hao Lin Chiu, “Degradation of the Capacitance-Voltage Behaviors of the Low-Temperature Polysilicon TFTs under DC stress,” Journal of The Electrochemical Society, 154 (7) H611-H618, 2007.